AD_____

Award Number: DAMD17-00-1-0385

TITLE: Regulation of Actin-Myosin Cytoskeletal Changes Involved in Cancer Metastasis

PRINCIPAL INVESTIGATOR: Teng-Leong Chew, Ph.D.

CONTRACTING ORGANIZATION: Northwestern University
Evanston, Illinois 60208-1110

REPORT DATE: July 2001

TYPE OF REPORT: Annual Summary

PREPARED FOR: U.S. Army Medical Research and Materiel Command
Fort Detrick, Maryland 21702-5012

REPORT DOCUMENTATION PAGE

Form Approved
OMB No. 074-0188

1. AGENCY USE ONLY (Leave blank)	2. REPORT DATE	3. REPORT TYPE AND DATES COVERED
	July 2001	Annual Summary (1 Jul 00 - 30 Jun 01)

4. TITLE AND SUBTITLE
Regulation of Actin-Myosin Cytoskeletal Changes Involved in Cancer Metastasis

5. FUNDING NUMBERS
DAMD17-00-1-0385

6. AUTHOR(S)
Teng-Leong Chew, Ph.D.

7. PERFORMING ORGANIZATION NAME(S) AND ADDRESS(ES)
Northwestern University
Evanston, Illinois 60208-1110

E-Mail: r-chisholm@northwestern.edu

8. PERFORMING ORGANIZATION REPORT NUMBER

9. SPONSORING / MONITORING AGENCY NAME(S) AND ADDRESS(ES)
U.S. Army Medical Research and Materiel Command
Fort Detrick, Maryland 21702-5012

10. SPONSORING / MONITORING AGENCY REPORT NUMBER

11. SUPPLEMENTARY NOTES
Report contains color

12a. DISTRIBUTION / AVAILABILITY STATEMENT
Approved for Public Release; Distribution Unlimited

12b. DISTRIBUTION CODE

13. ABSTRACT ***(Maximum 200 Words)***

This research is aimed to define the molecular events mediating tumor cell migration during metastasis. Although myosin is required for motility, how force is generated to initiate and maintain directed movement of non-muscle cells remains poorly understood. We have two approaches to elucidate myosin-based motility with high spatial and temporal resolution. Green fluorescent protein (GFP) tagged myosin II regulatory light chain (RLC) has allowed us to follow the reorganization of the myosin network during motility. Since RLC is regulated by multiple signals, further understanding of the signaling events cannot be accomplished without dynamic spatio-temporal dissection of the pathways. To accomplish this, we have generated a novel biosensor that allows us to simultaneously monitor the subcellular localization of myosin light chain kinase (MLCK) and its state of activation. we have characterized how myosin is regulated at various subcellular regions during cell motility. To establish a baseline for studies of breast cancer cells, we used PTK-2 epithelial cells to understand the role of myosin at the leading edge of motile cells. The MLCK-FIP biosensor has highlighted myosin function unlikely to be controlled. Our initial efforts have established the necessary techniques and the basic principles of MLCK-mediated non-muscle myosin regulation to characterize the fundamental differences in the acto-myosin cytoskeleton in non-invasive and the highly aggressive tumor breast cancer cells.

14. SUBJECT TERMS	15. NUMBER OF PAGES
	46
	16. PRICE CODE

17. SECURITY CLASSIFICATION OF REPORT	18. SECURITY CLASSIFICATION OF THIS PAGE	19. SECURITY CLASSIFICATION OF ABSTRACT	20. LIMITATION OF ABSTRACT
Unclassified	Unclassified	Unclassified	Unlimited

Table of Contents

INTRODUCTION

This research is aimed to define the molecular events mediating tumor cell migration during metastasis. Although myosin is required for motility, how force is generated to initiate and maintain directed movement of non-muscle cells remains poorly understood. We have two approaches to elucidate myosin-based motility with high spatial and temporal resolution. Green fluorescent protein (GFP) tagged myosin II regulatory light chain (RLC) has allowed us to follow the reorganization of the myosin network during motility. Since RLC is regulated by multiple signals, further understanding of the signaling events cannot be accomplished without dynamic spatio-temporal dissection of the pathways. To accomplish this, we have generated a novel biosensor that allows us to simultaneously monitor the subcellular localization of myosin light chain kinase (MLCK) and its state of activation. we have characterized how myosin is regulated at various subcellular regions during cell motility. To establish a baseline for studies of breast cancer cells, we used PTK-2 epithelial cells to understand the role of myosin at the leading edge of motile cells. The MLCK-FIP biosensor has highlighted myosin function unlikely to be controlled. Our initial efforts have established the necessary techniques and the basic principles of MLCK-mediated non-muscle myosin regulation to characterize the fundamental differences in the acto-myosin cytoskeleton in non-invasive and the highly aggressive tumor breast cancer cells.

BODY

During this funding period (starting from July 1, 2000), we have concentrate our effort on the first two specific aims in pursuing our ultimate goal of dynamically characterizing the differences in myosin regulation in non-invasive (MCF-7) and highly metastatic (MDA-MB231) breast cancer cells. The specific aims remain unchanged from the application.

Task 1 To characterize the dynamics of myosin regulation and remodeling during cell movement.

We have generated GFP-tagged RLC to characterize the dynamic organization of myosin II during cell motility. Previous result showed that GFP-RLC co-localized with myosin *in vivo* by immunolocalization. We have since proved that GFP-RLC co-immunoprecipitated with myosin II (Figure 1), indicating that GFP-RLC associates with myosin *in vivo*. GFP-tagged wt RLC can be phosphorylated to the same extent *in vivo* as endogenous RLC. These results indicate that GFP-RLC and provides a true representation of myosin dynamics.

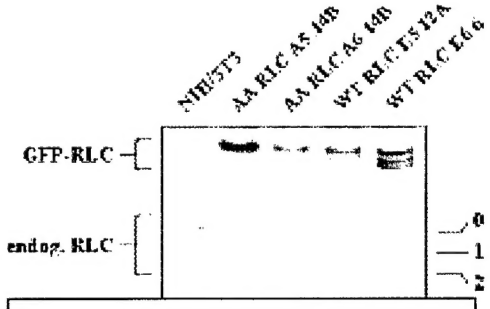

Figure 0 *Phosphorylation state of GFP-tagged RLCs co-immunoprecipitated with myosin heavy chain.*

Myosin was immunoprecipitated from NIH3T3 stably expressing GFP-tagged wt RLC or non-phosphorylatable RLC (AA). Proteins were analyzed on glycerol-urea gel and immunoblotted using anti-RLC antibody. 0, 1, and 2 denotes the phosphorylation state of RLC *in vivo*.

To establish a baseline for studies with tumor cells, we characterized the myosin organization. PtK-2 cells plated on fibrobectin-coated coverslips and stimulated to migrate with hepatocyte growth factor. Primary mouse embryonic fibroblasts also undergo rapid movement spontaneously. This initial characterization highlighted several important aspects of myosin reorganization. As reported previously, myosin assembles into bipolar filaments at the leading edge of the lamella. These bipolar filaments undergo further organization to form myosin ribbons that appear as spots moving toward the cell center. We have shown that myosin ribbons coalesce into stress fibers behind the lamella, forming a convergence zone where active myosin contraction ensues (2, 4). Rapid myosin contraction also pulls on the focal adhesion near the tail (6). Although the latter observation fits the model that myosin facilitates tail retraction, the role of myosin at the leading front is unclear. The state of RLC phosphorylation within the myosin ribbon remained uncharacterized when we proposed this study. We have shown that the lamella contains a gradient of increasing RLC phosphorylation from the leading edge to the cell center (7).

Task 2 To study the spatio-temporal involvement of MLCK in myosin remodeling.

As described in our application, we have been developing a novel MLCK biosensor that allows us to simultaneously detect the localization of MLCK and its state of activation in live cells. The binding of $[Ca^{2+}]_4$/calmodulin to the biosensor, MLCK-FIP, disrupts the fluorescent resonant energy transfer (FRET) between the BFP and GFP (6, 7).

Using MLCK-FIP, we have examined the regulation of myosin during various morphological changes. The results obtained thus far have greatly improved our understanding of how myosin activity and organization are regulated, and are presented at the 2001 Gordon Research Conference "Motile and Contractile System" section (6) and in the attached manuscript (7). This manuscript (Figure 4) shows that $MLCK_{125}$ activation and its recruitment to stress fibers precede contraction, an event in which MLCK activity has been implicated by numerous studies. The enrichment of $MLCK_{125}$ on stress fiber continues to increase during the course of contraction. Recent studies (1, 10) showed that the gene locus of MLCK in vertebrates generates three known proteins: (i) the ~108 – 125 kDa short MLCK ($MLCK_{125}$) that is found in smooth muscle and non-muscle cells; (ii) the ~210 kDa MLCK ($MLCK_{210}$) that is a differentially spliced isoform of the short MLCK expressed in non-muscle cells; (iii) and a enzymatically inactive

telokin which is identical to the C-terminal half of MLCK (1). This N-terminal extension greatly increases the affinity of $MLCK_{210}$, and preferentially targets it to stress fibers (1, 10). Since $MLCK_{210}$ remains stress fiber-bound, it is unclear why non-muscle cells need two isoforms of MLCK, both under the control of $[Ca^{2+}]_4$/calmodulin, to mediate myosin activity. Currently, the localization of $MLCK_{125}$ in non-muscle cells is debatable. Using GFP-tagged $MLCK_{125}$, Lin *et al.* have shown that $MLCK_{125}$ associates with stress fibers (9), contradicting the diffuse localization observed by Poperechnaya *et al.*(10). This discrepancy cannot be resolved by immunolocalization, since antibody against $MLCK_{125}$ will inevitably recognize $MLCK_{210}$. The MLCK-FIP construct is based on $MLCK_{125}$, and is perfectly suited to address this unresolved question.

Our data demonstrate that $MLCK_{125}$ localization is a transient event, thus reconciling the discrepancy of $MLCK_{125}$ localization in the literature. The association of $MLCK_{125}$ with stress fibers has been further confirmed with co-localization with rhodamine phalloidin stain. These data were presented at various meetings and in the attached manuscript (3, 6, 7).

In migrating cells, $MLCK_{125}$ is activated in the lamella, corresponding to increased RLC phosphorylation (Figure 3, manuscript). Recent advances have explained the fundamental principles actin polymerization as the driving force for lamellipodial protrusion. The finding of increased $MLCK_{125}$ activity at the leading front refocuses our attention to potential myosin function at the leading front. We have proposed a model of myosin works in synergy with actin polymerization at the leading front to facilitate directed cell movement. On the other hand, to our surprise, $MLCK_{125}$ at the trailing end is not activated to the same extent seen in the leading front. Although myosin activity is postulated to be involved in tail retraction, our results suggest that $MLCK_{125}$ may not be the kinase responsible for phosphorylating RLC at the tail. This finding is consistent with recent implication of Rho kinase in mediating tail retraction (11). More importantly, it demonstrates the capability of MLCK-FIP to not only pinpoint regions where $MLCK_{125}$ is active, but also highlight regions where myosin activity may not be regulated by $MLCK_{125}$. This fulfills one of the critical requirements for us to tackle the third specific aims in the proposed project: to characterize the crosstalk between signaling pathways leading to cytoskeletal changes.

In response to comments by reviewers of our application, we have also employed GFP-tagged paxillin and vinculin to study the dynamic interaction of myosin network and focal adhesion. Preliminary results have been presented as abstract at the ASCB meeting. Simultaneous localization of paxillin and myosin RLC showed that focal adhesions are assembled at the leading edge of motile cells, and that these nascent focal adhesions are not co-localized with the myosin ribbons. We have also observed that myosin sarcomeric units on stress fibers move away from focal contacts, raising the questions of whether this movement represents the treadmilling of actin filaments or myosin movement (2). If actin filaments treadmill from focal adhesion, then the microfilament-focal adhesion interaction has to be dynamic to allow for further actin polymerization to occur. If myosin is moving actin tracks, then how myosin can under unidirectional movement on actin filaments of mixed polarity has to be deciphered. We are in the process of determining the nature of this molecular event.

This improved understanding of myosin-mediated force generation now allows us to proceed to a detailed comparison of how myosin is organized and regulated in non-invasive and highly metastatic breast cancer cell. Similar experiments that performed thus far that have contributed to our understanding of myosin regulation will be performed on the breast cancer cells. Due to the recent discovered differentially spliced MLCK isoforms, we planned to also generate a similar biosensor to characterize the $MLCK_{210}$. With our experience in performing FRET analysis, we do not foresee any difficulty in this task.

KEY RESEARCH ACCOMPLISHMENTS:

- Biochemical analysis has demonstrated that our recombinant biosensors for myosin and $MLCK_{125}$ provide accurate representation of myosin and $MLCK_{125}$ function.

- Detailed characterization of myosin and focal adhesion organization and regulation during cell migration.
  - Myosin is organized into ribbons that undergo retrograde movement within extending lamella.
  - Extensive myosin contraction takes place between the lamella and the cell centroid, creating a "convergence zone" wherein myosin ribbon coalesce into stress fibers.
  - Nascent focal adhesions assemble at the leading edge of motile cells but do not co-localize with myosin ribbons.
  - Myosin forms large cortical bundles at the tail of moving cells, and active contraction at this region facilitate the disengagement of focal adhesion.
  - Myosin sarcomeric units stream away from focal contacts. The underlying mechanism is not known.

- Dynamic characterization of $MLCK_{125}$ localization and activation during various morphological changes.
  - $MLCK_{125}$ is activated within extending lamella.
  - Localized activation of $MLCK_{125}$ precedes regional cell contraction.
  - $MLCK_{125}$ is actively recruited to the shortening stress fibers during contraction.
  - During cell division, $MLCK_{125}$ enrichment at the midzone of mitotic spindle at late metaphase precedes its maximal activation.

- Refocusing attention to the neglected role of myosin contraction at the leading lamella of migrating cells.

- The general understanding of dynamic myosin function and regulation serving as the critical foundation for assessing motility as determining factor for metastatic potential.

REPORTABLE OUTCOMES

1. GFP-RLC indicates regions of contraction between lamella and nucleus during motility.

2. Capability of MLCK-FIP to accurately detect $MLCK_{125}$ binding to $[Ca^{2+}]_4$/calmodulin *in vivo.*

3. Activation of $MLCK_{125}$ precedes cell retraction.

4. $MLCK_{125}$ is transiently recruited to stress fibers during contraction.

5. MLCK-FIP highlights regions of RLC phosphorylation.

6. $MLCK_{125}$ is activated in the lamella during cell protrusion.

7. GFP-paxillin showed the disassembly of focal adhesion during cytokinesis.

8. MLCK-FIP shows bimodal distribution of $MLCK_{125}$ activity during cytokinesis – similar to the distribution of myosin.

CONCLUSIONS

Myosin regulation is mediated by multiple signals. The convergence of these pathways on the same residue of myosin II RLC necessitates a novel approach with high spatiotemporal resolution. Data obtained thus far carries numerous critical implications. We have correlated the dynamic myosin organization during cell motility with the distribution of $MLCK_{125}$ activity. Our biosensor highlighted a previously unidentified function of $MLCK_{125}$ in phosphorylating loosely assembled myosin to facilitate subsequent organization into large myosin network. This result, coupled with our finding of active myosin contraction at the leading front has refocused our attention to the potential role played by myosin at the convergence zone in front of the nucleus.

We have also shown that $MLCK_{125}$ localization to the stress fibers is a transiently controlled event. This observation provides evidence to reconcile a previous discrepancy of $MLCK_{125}$ localization in the literature. It also addressed one of the questions we proposed in the application with regards to the dynamics of MLCK in regulating the physiology of stress fibers. We have probed the sequence of events leading to stress fiber shortening, and confirmed that $MLCK_{125}$ activation preceded cell contraction. In addition, there was an active recruitment of $MLCK_{125}$ to the stress fibers during contraction.

We have thus far addressed some the fundamental questions we hoped to answer: (1) How is myosin organized to facilitate directed movement? and (2) How do migrating cells target myosin and MLCK activity for proper locomotion? These findings form the foundation on which subsequent experiments are based to assess the features of motility that can serve as a determining factor for metastatic potential. We are also in the process of generating CFP-tagged α-catenin to allow for dynamic monitoring of the interaction between acto-mysoin system and cell-cell adhesion. This improved understanding of the mechanism of myosin regulation and function during morphological changes now allows us to proceed to the second of phase of the proposed research to compare the motility in MCF-7 and MDA MB-231.

REFERENCES

1. Birukov, K. G., Schavocky, J. P., Shirinsky, V. P., Chibalina, M. V., Van Eldik, L. J., and Watterson, D. M. (1998). Organization of the genetic locus for chicken myosin light chain kinase is complex: multiple proteins are encoded and exhibit differential expression and localization. J Cell Biochem *70*, 402-13.

2. Wolf W. A., Chew, T. L. and Chisholm R. L. GFP-labeled myosin RLC allows direct visualization of stress fibers contraction in live cells. Mol. Biol. Cell *10S*: 131a, 1999

3. Chew T. L. Wolf, W. A., Gallagher, P. J., and Chisholm R. L. Regional activation of MLCK correlates with morphological changes in live cells. Mol. Biol. Cell *10S*: 379a, 1999

4. Chew, T. L., Wolf, W. A., and Chisholm R. L. Imaging of GFP-tagged cytoskeletal proteins in live cells provides a means of assessing the effects of surfaces on cell behavior. *Materials Research Society. Symposium DD: Interfacial Aspects of Soft Biomaterials.* April 2000

5. Chew, T.-L., Wolf, W.A., Gallagher, J. A., Matsumura, F., and Chisholm, R. L. The enrichment of myosin light chain kinase at the cleavage furrow precedes its activation. Mol. Biol. Cell *11S,* 563a, 2000

6. Chew, T.-L., Wolf, W.A., Gallagher, J. A., Matsumura, F., and Chisholm, R. L. A FRET-based biosensor reveals compartmentalization of myosin light chain kinase activity during morphological changes *Gordon Research Conference:Motile and Contractile Systems.* June, 2001

7. Chew, T.-L., Wolf, W.A., Gallagher, J. A., Matsumura, F., and Chisholm, R. L. A FRET-based biosensor reveals compartmentalized interaction of myosin light chain kinase and $[Ca^{2+}]_4$/calmodulin. (manuscript submitted.

8. Gallagher, P. J., and Herring, B. P. (1991). The carboxyl terminus of the smooth muscle myosin light chain kinase is expressed as an independent protein, telokin. J Biol Chem *266*, 23945-52.

9. Lin, P., Luby-Phelps, K., and Stull, J. T. (1997). Binding of myosin light chain kinase to cellular actin-myosin filaments. J Biol Chem *272*, 7412-20.

10. Poperechnaya, A., Varlamova, O., Lin, P., Stull, J. T., and Bresnick, A. R. (2000). Localization and activity of myosin light chain kinase isoforms during the cell cycle. J Cell Biol *151*, 697-708.

11. Worthylake, R. A., Lemoine, S., Watson, J. M. and Burridge, K. (2001) RhoA is required for monocyte tail retraction during transendothelial migration. J Cell Biol. 154: 147-160.

A FRET-based biosensor reveals compartmentalized interaction of myosin light chain kinase and $[Ca^{2+}]_4$/calmodulin.

Teng-Leong Chew, Wendy A. Wolf, Patricia J. Gallagher, Fumio Matsumura,
and Rex L. Chisholm.

Department of Cell and Molecular Biology and the R. H. Lurie Comprehensive Cancer Center, Northwestern University Medical School, Chicago, IL 60611;

[1] Department of Physiology, Indiana University School of Medicine, Indianapolis, IN 46202;

[2] Department of Molecular Biology and Biochemistry, Rutgers University, Nelson Labs, Busch Campus, Piscataway, NJ 08855

SUMMARY

Multiple signaling cascades converge on the regulatory light chain of nonmuscle myosin II. An approach with high spatial and temporal resolution is thus required to dissect how these signals mediate myosin activity. Using temporally and spatially resolved fluorescence resonance energy transfer (FRET), we have developed a novel biosensor that can simultaneously detect the subcellular localization of MLCK as well as its dynamic $[Ca^{2+}]_4$/calmodulin-binding state in live cells. Using the biosensor, we have made the following observations: (1) A transient elevation from a low but detectable basal MLCK activity precedes cellular contraction, (2) MLCK is actively recruited to the stress fibers during contraction, (3) MLCK is active at the lamellipodia of migrating cells, implicating the kinase as a regulator of myosin activity in the lamella, (4) During cytokinesis, MLCK is enriched at the spindle equator at late metaphase, but the maximal activation occurs just prior to the onset of cleavage furrow constriction, (5) Active MLCK is redistributed to the poles of the daughter cells toward the end of cytokinesis. This biosensor will serve as a critical tool for further deciphering how cells compartmentalize the MLCK signals during active morphological changes.

INTRODUCTION

Phosphorylation of the 20 kDa regulatory light chain (RLC) is critical for the regulation of non-muscle myosin II. The RLC phosphorylation sites can be categorized into two groups by their effects on myosin function. Ser-19 and Thr-18 are the two stimulatory sites, while Ser-1, Ser-2 and Thr-9 are inhibitory to myosin activity when phosphorylated. Ser-19 is targeted by myosin light chain kinase (Ikebe et al., 1986; Sellers et al., 1981), Rho kinase (Amano et al., 1996), and p21-activated kinase (PAK) (Chew et al., 1998; Zeng et al., 2000). MLCK can further phosphorylate RLC at Thr-18 at high *in vitro* concentration (Ikebe et al., 1986). The diphosphorylation of Ser-19 and Thr-18 maximally activate the myosin ATPase activity *in vitro* (Sellers et al., 1981). This is consistent with the results that maximal isometric tension development in thrombin-stimulated endothelial cells correlates with Ser-19 and Thr-18 phosphorylation (Goeckeler and Wysolmerski, 1995). Ser-1, Ser-2 and Thr-9 of RLC, when phosphorylated by protein kinase C (Ikebe et al., 1987) and Cdc2 kinase (Mishima and Mabuchi, 1996; Satterwhite et al., 1992), inhibit myosin activity as well as decrease the Km of MLCK for RLC (Turbedsky et al., 1997).

The RLC-targeting kinases are regulated by distinct upstream signals ranging from $[Ca^{2+}]_4$/calmodulin to Rho family GTPases. As disparate as these pathways are, many of them exhibit crosstalk. The Cdc42-mediated PAK, for example, monophosphorylates RLC at Ser-19

(Chew et al., 1998; Zeng et al., 2000), yet it prevents MLCK (Goeckeler and Wysolmerski, 1995; Sanders et al., 1999) from diphosphorylating RLC at Ser-19 and Thr-18. We have yet to unravel why a plethora of signals is required to target the same residues in RLC. Taken together, these data indicates that cells can compartmentalize their signals both spatially and temporally and that signal transduction cannot be considered in simple, linear terms. It is unclear how these kinases are targeted to the proper sites of action. This question remains unresolved due to our inability to detect these molecular events dynamically.

MLCK is a $[Ca^{2+}]_4$/calmodulin-dependent kinase implicated in cell contraction (Garcia et al., 1995; Goeckeler and Wysolmerski, 1995), cytokinesis (Poperechnaya et al., 2000), stress fiber formation (Chrzanowska-Wodnicka and Burridge, 1996), and motility (Kishi et al., 2000). Although previous immunolocalization studies have localized MLCK to stress fibers as well as cleavage furrow of dividing cells (de Lanerolle et al., 1981; Guerriero et al., 1981), the activation state of MLCK in these locations was unclear. The formation and maintenance of stress fibers require the phosphorylation of RLC (Chrzanowska-Wodnicka and Burridge, 1996), and is consistent with the association of MLCK with stress fiber. Localization of MLCK to stress fiber, however, does not explain why myosin is not therefore fully activated leading to maximal cell contraction. It also raises the question of whether myosin has to be further activated before maximal contraction ensues. In addition, it remains to be elucidated if MLCK activation precedes its localization to stress fibers. The convergence of multiple signals on myosin highlights the possibility of regionalized myosin regulation by distinct pathway. Taken together, these unresolved issues underscore the need to spatially and temporally dissect the pathways. As the best characterized RLC-targeting kinase, MLCK serves as an ideal first candidate toward accomplishing this goal.

Taking advantage of the fluorescent resonant energy transfer (FRET) between the blue (BFP) and the green (GFP) fluorescent proteins, Romoser *et al.* developed a fluorescent indicator protein (FIP) that detects $[Ca^{2+}]_4$/calmodulin changes in living cells (Romoser et al., 1997). Here we report the engineering of a novel biosensor by fusing the FIP to the C-terminus of MLCK (Figure 1). The resulting construct now allows us to dynamically detect the co-localization of MLCK with $[Ca^{2+}]_4$/calmodulin, a molecular event critical for the kinase activation. Using this approach, we show that localized MLCK activation along stress fibers precedes cell contraction, demonstrating that MLCK activity can be modulated *in situ* on stress fibers to mediate the extent of myosin contractility. MLCK is also activated within the protruding lamella. This finding places MLCK at the precise subcellular region to mediate RLC phosphorylation important for myosin organization. During cell division, MLCK displays a bimodal distribution. Its

enrichment at the spindle equator occurs at metaphase, which precedes its maximal activation at the onset of cleavage furrow contraction. Immediately before the formation of midbody, MLCK activity is distributed toward the polar ends of the two daughter cells. Detailed spatial and temporal characterization of signaling mechanism confirms the hypothesized compartmentalization of MLCK *in vivo*, and helps highlight regional myosin activities that may not involves MLCK for further studies.

RESULTS

MLCK-FIP as a detector of MLCK co-localization with $[Ca^{2+}]_4$/calmodulin.

The 56 kDa FIP consists of a BFP linked to a GFP via a $[Ca^{2+}]_4$/calmodulin-binding domain derived from MLCK. In the absence of $[Ca^{2+}]_4$/calmodulin, the coiled conformation of the $[Ca^{2+}]_4$/calmodulin-binding domain (CBD) linking the two fluorophores facilitates FRET between BFP and GFP, if BFP is excited (Figure 1A) (Romoser et al., 1997). If the MLCK-FIP encounters high $[Ca^{2+}]_4$/calmodulin concentration in the cell, where MLCK will be activated, $[Ca^{2+}]_4$/calmodulin will bind not only to MLCK, but also in between the two fluorophores. The binding of CaM changes the conformation of the CBD, increasing the distance between the two fluorophores, disrupting the FRET. By exciting BFP and monitoring the emission from GFP, we can therefore dynamically monitor the subcellular localization and the activation state of MLCK.

The gene locus of MLCK in vertebrates generates three known proteins (Birukov et al., 1998): (i) the ~108 – 125 kDa short MLCK ($MLCK_{125}$) that is found in smooth muscle and non-muscle cells; (ii) the ~210 kDa MLCK ($MLCK_{210}$) that is a differentially spliced isoform of the short MLCK expressed in non-muscle cells; (iii) and a enzymatically inactive telokin which is identical to the C-terminal half of MLCK (Gallagher and Herring, 1991). $MLCK_{210}$ is expressed predominantly in non-muscle cells, and possesses an extension at the N-terminus that comprises of more than 900 residues (Poperechnaya et al., 2000). This N-terminal extension greatly increases the affinity of $MLCK_{210}$, and preferentially targets it to stress fibers (Poperechnaya et al., 2000). The localization of $MLCK_{125}$ is currently debatable. Since antibody raised against $MLCK_{125}$ inevitably recognizes $MLCK_{210}$, we cannot derive conclusion from previous immunolocalization studies. Using GFP-tagged $MLCK_{125}$, Poperechnaya *et al.* and Lin *et al.* showed that $MLCK_{125}$ displays different localization in different cell types (Lin et al., 1999; Poperechnaya et al., 2000). Since $MLCK_{210}$ remains stress fiber-bound, it is unclear why non-muscle cells need two isoforms of MLCK, both under the control of $[Ca^{2+}]_4$/calmodulin, to mediate myosin activity. These unresolved issues clearly necessitate further dynamic characterization of $MLCK_{125}$. We have chosen therefore to characterize $MLCK_{125}$ by FIP fusion.

MLCK-FIP displays $[Ca^{2+}]_4$/calmodulin-dependent kinase activity comparable to wt MLCK.

To determine whether the FIP tag interfered with MLCK regulation, we tested its ability to phosphorylate RLC *in vitro.* Lysates from COS-7 cells over-expressing either wild type MLCK or MLCK-FIP were incubated with recombinant RLC. In the presence of $[Ca^{2+}]_4$/calmodulin, the kinase activities from lysates containing recombinant wt MLCK or MLCK-FIP are significantly higher than that found in lysate of mock-transfected cells, ruling out the possibility that the

kinase activities we observe are contributed by the endogenous MLCK. Figure 1B demonstrates that MLCK-FIP retains $[Ca^{2+}]_4$/calmodulin-dependent activity to phosphorylate RLC to comparable extent as that of wild type MLCK, indicating that the FIP tag does not interfere with the regulation of MLCK.

To confirm that the FIP does not affect the kinase activity, we compared the rates of RLC phosphorylation mediated by MLCK-FIP and wt MLCK at three substrate concentrations. This approach is necessary because the bacterially expressed RLC tended to precipitate at high concentration, limiting our ability to rigorously determine the Km and Vmax. MLCK-FIP or wt MLCK were over-expressed in COS-7 cells and immunoprecipitated using pAb against MLCK and the amount of recombinant MLCK-FIP and wt MLCK is estimated by comparing their intensity on an immunoblot to that of a standard curve (Figure 1C, bottom panel). The fact that we cannot detect endogenous kinase in our immunoblot indicates that the immunoprecipitates are representative of the recombinant kinase activity (a faint endogenous band of $MLCK_{125}$ was evident only after prolonged exposure, data not shown). Immunoprecipitates containing equal amount of wt MLCK and MLCK-FIP were used in the *in vitro* kinase assay. Figure 1C shows that both wt MLCK and MLCK-FIP phosphorylates RLC at indistinguishable rate at all three substrate concentrations tested. Since our recombinant RLC is buffered in high salt concentration to prevent precipitation, it is interesting to note that in all cases both wt MLCK and MLCK-FIP only monophosphorylate RLC (~1 mole phosphate incorporated per mole RLC). This is consistent with previous findings that the MLCK-mediated diphosphorylation of RLC is sensitive to high ionic strength (Ikebe and Hartshorne, 1985). Taken together, these data demonstrate that MLCK-FIP has the same $[Ca^{2+}]_4$/calmodulin-dependent kinase activity as wt MLCK.

MLCK-FIP detects $[Ca^{2+}]_4$/calmodulin *in vitro*.

Next, we ascertained the ability of MLCK-FIP to detect $[Ca^{2+}]_4$/calmodulin changes *in vitro*. MLCK-FIP was purified, and the protein was assayed as described. Increasing amounts of $CaCl_2$ were added and the sample was excited at 380 nm and the emission spectra from 430 nm to 550 nm obtained. As shown in Figure 2A, MLCK-FIP displays a corresponding decrease in FRET as detected by the emission peak of 509 nm in response to increasing $[Ca^{2+}]_4$/calmodulin concentration. The drop in GFP emission is also accompanied by a corresponding increase in BFP emission, indicative of a true FRET spectrum. This result is consistent with previously published behavior of FIP (Romoser et al., 1997), thus demonstrating that MLCK-FIP maintains the functionality to detect $[Ca^{2+}]_4$/calmodulin changes. The fact that

MLCK-FIP does not lose the FRET signal in the presence of calmodulin when there is no free Ca^{2+} indicates that the biosensor does not detect inactive calmodulin.

Obtaining FRET ratio images *in vivo*.

The relative state of MLCK activation is determined by ratio imaging. Previous study performed ratio imaging using the F_{448}/F_{510} ratio, which is the ratio of fluorescent intensity of BFP to that of GFP (Romoser et al., 1997). In the presence of CaM, FRET is disrupted, increasing the fluorescent intensity of BFP while decreasing that of GFP, thus causing the F_{448}/F_{510} ratio to drop. The F_{488}/F_{510} therefore will provide a representation of MLCK relative activity as monitored by MLCK-FIP. However, specific targeting mechanisms most likely localize MLCK to specific sites within the cell. This specific localization requires an independent method to determine the intensity of MLCK, which may provide clues to dynamic MLCK recruitment or redistribution.

Since the fluorescent intensities of BFP and GFP change in inverse proportion to one another, as shown in Figure 3 (fluorescent intensity of BFP decreases when GFP increases, and vice versa), the ratio of F_{448}/F_{510} provides no constant internal control, and cannot be used to determine the relative amount of MLCK-FIP in any given region of the cell. We have developed an alternative approach to obtain ratio images. The numerator of the ratio (F_{FRET}) is obtained by exciting BFP at 380 nm, and measuring GFP emission at 510 nm, thus corresponding to the GFP emission as a result of FRET. The denominator (F_{GFP}) is obtained by directly exciting the GFP at 460 nm and measuring the emission at 510 nm. Since F_{GFP} is obtained by direct excitation of the GFP, the fluorescent intensity does not change regardless of the degree of FRET between BFP and GFP, therefore providing an independent measurement of MLCK localization. The ratio images were then presented on a ratio bar such as that in Figure 4 using Intensity Modulated Display (IMD) (Tsien and Harootunian, 1990), which uses ratio to determine color hue, but utilizes the intensity from wavelength images to determine the intensity of the color hue. Since the loss of FRET signal indicates the co-localization of MLCK-FIP and $[Ca^{2+}]_4$/calmodulin, the low ratio (blue end of the ratio bar) signifies relatively higher activity, and vice versa. Based on the intensity of the denominator image, the ratio color is then displayed in the corresponding intensity.

The 256 pixel values (0-255) are therefore representations of 16 different relative activity units with 16 distinct intensity levels. This mathematical manipulation allows us to separate the relative activity from the intensity profile in any given region of the cell, and provides a dynamic two-dimensional display of MLCK regulation.

MLCK-FIP detects $[Ca^{2+}]_4$/calmodulin changes *in vivo*.

To test MLCK-FIP functionality in live cells, MLCK-FIP spectra were monitored following Ca^{2+} ionophore ionomycin treatment of COS-7 cells transiently transfected with the biosensor. COS-7 cells were chosen strictly for their capability to significantly over-express recombinant proteins and high transfection efficiency. As shown in Figure 2B, the high protein expression level resulted in a generally diffuse localization of MLCK-FIP. Prior to the ionomycin treatment, ratio images indicates that MLCK-FIP was not in the $[Ca^{2+}]_4$/calmodulin-bound state (red, MLCK inactive). A dramatic time-dependent loss of FRET occurs immediately after ionomycin treatment (Figure 2B, and movie clip 2B), turning all imaged cells to green or blue, indicating that MLCK-FIP has bound $[Ca^{2+}]_4$/calmodulin (MLCK active). This result clearly shows that MLCK-FIP detects $[Ca^{2+}]_4$/calmodulin changes in live cells. It should also be noted that MLCK-FIP detected increased $[Ca^{2+}]_4$/calmodulin binding without exogenously added calmodulin even when MLCK-FIP was over-expressed.

MLCK-FIP localizes to stress fibers and implicates MLCK activity in subcellular regions of RLC phosphorylation.

Since MLCK-FIP localizes $MLCK_{125}$ activity to stress fibers during contraction where myosin is postulated to be active, the biosensor should accurately pinpoint regions with elevated RLC phosphorylation. To test this, we compared the MLCK-FIP ratio image with the distribution of phosphorylated RLC using pAb specific for RLC phospho-Ser-19. In order to highlight regions with elevated myosin phosphorylation, the level of RLC phosphorylation was displayed as a ratio to total myosin (Figure 3A, right panel). PTK-2 cells expressing MLCK-FIP was imaged to obtain a F_{FRET}/F_{GFP} ratio (Figure 3A, left panel) and immediately fixed and double-stained for myosin heavy chain and phosphorylated RLC. Ratio of the phosphorylated RLC to total myosin is constructed using MetaMorph 4.5 software.

Figure 3A shows, as expected, elevated RLC phosphorylation along stress fibers. There are also regions such as the lamellipodia where RLC shows a gradient of increasing phosphorylation toward the cell center. Since the antibody specific for phosphorylated RLC has a higher affinity for mono-phosphorylated RLC than the diphosphorylated form (Matsumura et al., 1998), it was possible that the extent of RLC phosphorylation was under-estimated. Overall, F_{FRET}/F_{GFP} ratio image shows that there is a strong correlation between $MLCK_{125}$ activation and RLC phosphorylation *in vivo*. Interestingly, MLCK-FIP indicates that MLCK is active within the lamellipodia of the cell where very few myosin structures are observed. Myosin is well documented to organized into nascent clusters of bipolar filaments which appears as spots that

undergo retrograde movement in the lamellipodia (Verkhovsky and Borisy, 1993; Verkhovsky et al., 1995). The *de novo* myosin organization within the lamellipodia is possible only if there is a pool of diffuse myosin to be targeted for regulation. RLC phosphorylation has been implicated by numerous *in vitro* studies to mediate myosin assembly into bipolar filaments. Ultrastructural analysis showed that myosin spots are clusters of bipolar filaments. The role of RLC phosphorylation in bipolar filament clustering has not been explored. The fact that the biosensor indicates that $MLCK_{125}$ is active within the lamellipodia ($n > 25$) places $MLCK_{125}$ at the precise location to mediate this event.

Figure 3A also highlighted the stress fiber localization of $MLCK_{125}$. This results contradict previous localization studies which showed that $MLCK_{125}$ is diffuse in the cytoplasm. In order to confirm that the stress fiber localization of $MLCK_{125}$, we performed co-localization of MLCK-FIP and rhodamine phalloidin. Figure 3B clearly shows the $MLCK_{125}$ stress fiber association.

Localized MLCK activation precedes cell contraction.

MLCK activation has been implicated in cell contraction (Garcia et al., 1995; Goeckeler and Wysolmerski, 1995) and directly correlates with isometric tension development in permeabilized endothelial cells (Wysolmerski and Lagunoff, 1991). We examined how MLCK activation correlated with cell contraction using MLCK-FIP. In order to characterize the dynamic redistribution of $MLCK_{125}$, we transiently transfected PTK-2 cells with the pcDNA3/MLCK-FIP. PTK-2 cells were selected for their high transfection efficiency, prominent stress fiber network, and much lower protein expression level compared to COS-7 cells, whose ultra-high expression level may interfere with the imaging of cytoskeletal structures. To better assess the $MLCK_{125}$ activity and localization, we displayed the ratio images using their intensity profiles. The actual intensity of MLCK-FIP is represented by the F_{GFP} image (denominator image). An intensity profile can be built by representing each pixel of the F_{GFP} image using a line the height of which corresponds proportionately with the pixel intensity. A region enriched with MLCK-FIP will therefore be represented by higher peaks. We then pseudo-colored the lines according to the F_{FRET}/F_{GFP} ratio bar (Figure 3, bottom panel).

We dissected the $MLCK_{125}$ signals during contraction using this method. Panels A-D in Figure 4 (and movie clips 4a) show that transient and highly localized $MLCK_{125}$ enrichment and activation on stress fibers precedes cellular contraction. It is important to note that the diffuse $MLCK_{125}$ (panel A) shows a dramatic redistribution prior to contraction by rapidly associating with stress fibers (arrow, panels B and C). $MLCK_{125}$ also exhibited the potential to be regulated *in situ* along stress fibers (arrow heads, panels B-D), where the activity first increased at the

early phase of contraction, then decreased. Panels E – H (movie clip 4b) confirm that the $MLCK_{125}$ activity and localization along stress fibers increase during contraction. More importantly these results show that $MLCK_{125}$ can associate with stress fiber, although it is likely that its association with the cytoskeleton may be more transiently controlled than that of $MLCK_{210}$.

$MLCK_{125}$ is activated in the lamellipodia of migrating cells.

Localization of $MLCK_{125}$ activity within the lamella dictates that the kinase should be activated in the extending lamellae of migrating cells. We therefore characterize the behavior of $MLCK_{125}$ using MLCK-FIP in hepatocyte growth factor/scatter factor-induced motile PTK-2 cells. Figures 5 shows representative image series (n = 9) of MLCK-FIP profile in motile PTK-2 cells. Consistent with the finding that $MLCK_{125}$ is active within lamellae of stationary cells, the kinase is activated also in the lamellae of migrating cells. Since the numerator F_{FRET} image and the denominator F_{GFP} image are taken sequentially using filter wheel, it is possible that the migrating cells may create a motion artifact which can be misinterpreted as a loss of FRET (hence the activation of MLCK). However, several lines of evidence argue against this. First, extending lamellipodia continue to show active MLCK-FIP (Figure 4) even after fixation. Second, alternating the order with which the numerator and denominator images are collected does not alter the MLCK-FIP activation profile (date not shown).

Lower protein expression level in PTK-2 cells also indicates that MLCK-FIP is not diffuse in the lamella, but apparently associates with actin-like filaments, consistent with previous finding that $MLCK_{125}$ binds filamentous actin. To our surprise, the relative level of $MLCK_{125}$ activation is consistently higher at the leading lamella than the retracting tail (8 out of 9 cells observed), where myosin contractility has been postulated to dislodge focal adhesions during cell movement. Previously published (Matsumura et al., 1998) and our current ratio images of phosphorylated RLC/total myosin clearly indicated elevated RLC phosphorylation at the tail. Our results suggest that MLCK-FIP may not be the kinase phosphorylating RLC at the tail, and therefore pinpoint the trailing tail to be a subcellular region controlled by signaling molecules other than $MLCK_{125}$.

$MLCK_{125}$ exhibits biphasic regulation during cytokinesis.

The myosin network undergoes dramatic reorganization during cell division. Previous data have shown that phosphorylated RLC is enriched in the midzones of separating chromosomes during late anaphase (Matsumura et al., 1998), prior to the constriction of

cleavage furrow. Poperechnaya *et al.* showed that $MLCK_{210}$ localized specifically to the cleavage furrow, as well as the cortical region of the dividing cell, whereas $MLCK_{125}$ remains diffuse (Poperechnaya et al., 2000). Thus, both the RLC phosphorylation and the activity of MLCK are tightly regulated during cell division.

Using MLCK-FIP, we have characterized the behavior of $MLCK_{125}$ during cytokinesis in transiently transfected NRK cells. NRK cells remain well attached to the substratum during cytokinesis, thus making it an ideal cell line to examine cytoskeletal changes during cell division. To evaluate changes in $MLCK_{125}$ activity during cytokinesis, we performed detailed pixel value analysis on three important subcellular regions. Region 1 represents the midzone of the mitotic spindle, Region 2 is immediately outside of the chromosomes, and region 3 represents the polar zone of the dividing cell (Figure 6). Due to the constant shape change we cannot confidently pinpoint the same pixel with respect to the dividing cell, so a region of 10 X10 pixel is selected in the mentioned regions, and the average pixel values are used to derive the intensity and activity profile presented on Figure 6 (bottom panel). MLCK-FIP is enriched at the equator of the mitotic spindle at late metaphase, the biosensor indicates that $MLCK_{125}$ is active but not maximally in this region. Immediately before the constriction of the cleavage furrow, $MLCK_{125}$ is maximally activated. Interestingly, this surge of activity is immediately followed a redistribution of active $MLCK_{125}$ to the polar regions of the two daughter cells. The remaining $MLCK_{125}$ at the cleavage continue to sustain the maximal activation state. MLCK at the polar region remain highly activated especially within the lamellipodia and ruffles. There is a noticeable drop in MLCK activity at the conclusion of cytokinesis when MLCK reverse back to partial activation state (green).

DISCUSSION

The convergence of multiple signals on RLC necessitates approaches with high spatio-temporal resolution to decipher myosin regulation. MLCK is a $[Ca^{2+}]_4$/calmodulin-dependent kinase. Therefore, a sensor that detects the $[Ca^{2+}]_4$/calmodulin-binding state of MLCK will indicate its activation state. We report here the generation and characterization of a FRET-based biosensor that allows us to simultaneously detect the localization of MLCK as well as its $[Ca^{2+}]_4$/calmodulin-binding state *in vivo*. Biochemical analyses show that MLCK-FIP phosphorylates RLC in a $[Ca^{2+}]_4$/calmodulin-dependent manner, while retaining the capability of the FIP to detect $[Ca^{2+}]_4$/calmodulin changes *in vitro* and *in vivo*, thus making MLCK-FIP a functional biosensor to monitor $MLCK_{125}$ regulation.

Potential limitation of MLCK-FIP

MLCK-FIP is built based on the assumption that if $MLCK_{125}$ binds to $[Ca^{2+}]_4$/calmodulin, it will be activated. The fact that $MLCK_{125}$ and FIP exhibit highly comparable $K_{calmodulin}$ (Romoser et al., 1997) suggests that FIP can closely reflect the $[Ca^{2+}]_4$/calmodulin-associated state of $MLCK_{125}$. There is, however, an important caveat. MLCK can be phosphorylated by numerous kinases at various serine residues. Based on initial phospho-peptide mapping, two residues have been designated as sites A and B, which correspond to Ser-815 and Ser-828 in gizzard smooth muscle kinase. Sites A and B are equivalent to Ser-992 and Ser-1005 in $MLCK_{125}$ used in the MLCK-FIP construct, respectively. Phosphorylation of site B has no detectable effect on MLCK (Nishikawa et al., 1985; Payne et al., 1986). Phosphorylation of site A by calmodulin-dependent kinase II or cAMP-dependent kinase increases the $K_{calmodulin}$ of $MLCK_{125}$ without affecting its Vmax (Ikebe and Reardon, 1990; Payne et al., 1986; Tansey et al., 1992). Since site A is located within the $[Ca^{2+}]_4$/calmodulin binding domain of MLCK, prior binding of $[Ca^{2+}]_4$/calmodulin attenuates phosphorylation at this residue. MLCK can also be phosphorylated by PAK at residues Ser 439 and Ser-991 in $MLCK_{125}$ (Goeckeler et al., 2000). Ser-439 has been postulated to affect protein-protein interaction. Since Ser-991 is adjacent to site A (Ser-992), thus binding of $[Ca^{2+}]_4$/calmodulin to MLCK also blocks PAK-mediated phosphorylation of Ser-991 (Goeckeler et al., 2000). Surprisingly, PAK phosphorylation reduces the V_{max} of MLCK, but not its $K_{calmodulin}$ (Sanders et al., 1999). The equivalents of Ser-991 and Ser-992 are present in the $[Ca^{2+}]_4$/calmodulin-binding sequence of FIP, although it is unclear if these residues will be regulated in similar fashion *in vivo*. Taken together, these kinases can potentially render MLCK-FIP prone to false positive signal, in which the FIP will display the kinase as active due to its binding with $[Ca^{2+}]_4$/calmodulin, when $MLCK_{125}$ is actually inactive. In

addition, treating the cells with inhibitors that target the MLCK nucleotide binding domain, such as KT-5926, would not change the MLCK-FIP $[Ca^{2+}]_4$/calmodulin binding, which may again be registered as a false positive signal. We do not have any means to eliminate this problem at this point. One way to improve accuracy of the MLCK-FIP read-out would be to probe for the dynamic localization of MLCK-targeting kinases while studying MLCK. Despite these limitations, MLCK-FIP remains the best tool available to study the dynamic regulation of MLCK *in vivo*. Using MLCK-FIP, we have characterized the regulation of $MLCK_{125}$ during various cellular events and have made the following observations.

Transient enrichment of active $MLCK_{125}$ induces contraction.

Although MLCK has been directly implicated in mediating cellular contraction in permeabilized endothelial cells (Wysolmerski and Lagunoff, 1991) and isolated stress fibers (Katoh et al., 2001), the dynamic aspects of how MLCK regulates myosin function is still poorly understood. $MLCK_{210}$ is known to associate with stress fibers with high affinity (Poperechnaya et al., 2000), suggesting that this MLCK isoform can be readily activated *in situ*. The dynamic myosin regulation by $MLCK_{125}$, however, is less well understood. It is unclear, for example, if the localization of $MLCK_{125}$ can be transiently controlled to allow for higher affinity toward the cytoskeleton when activated. Using GFP-$MLCK_{125}$, Poperechnaya *et al.* showed $MLCK_{125}$ to be largely diffuse in the cytoplasm, while Lin *et al.* observed filament-bound $MLCK_{125}$ (Lin et al., 1997; Lin et al., 1999; Poperechnaya et al., 2000). These discrepancies cannot be resolved by immunolocalization, as anti-$MLCK_{125}$ antibody will inevitably recognize $MLCK_{210}$. It also raises the question of whether the discrepancies arise from the different cell types used in the studies, or because the association of $MLCK_{125}$ to stress fibers is a more transient event.

Analysis of the MLCK-FIP ratio images reveals a two-fold regulation of $MLCK_{125}$ during active contraction. First, MLCK-FIP clearly shows that $MLCK_{125}$ interacts with stress fiber. In fact during the course of contraction, $MLCK_{125}$ is recruited to the stress fiber, supporting the notion that $MLCK_{125}$ localization to the cytoskeleton may be transient. There is also detectable amount of $MLCK_{125}$ associating with stress fibers prior to contraction, although their relative activity is low. $MLCK_{125}$ activation occurred prior to contraction, coincident with its recruitment to the stress fibers. Both $MLCK_{125}$ activity and intensity continued to increase at the initial phase of contraction as indicated by the ratio color shift to the low ratio range (blue), and the continual increase in intensity peaks along multiple stress fibers.

Rho kinase has been proposed (Katoh et al., 2001) to induce a slow but more sustainable contractility to maintain tension along stress fibers, whereas MLCK mediates a rapid

but transient contraction. This rapid enrichment of $MLCK_{125}$ activity on stress fibers is consistent with the published kinetic data. The Km of MLCK for RLC is higher than Rho kinase, suggesting that it may work optimally at high local RLC concentration. The high Vmax of MLCK makes it the ideal kinase to mediate rapid myosin activation. Our analysis of $MLCK_{125}$ clearly shows this dynamic behavior, wherein the rapid contraction induced by MLCK is enhanced by the local enrichment and activation of the kinase.

RLC phosphorylation in the lamella.

Previous *in vitro* biochemical studies show that RLC phosphorylation mediates myosin assembly into bipolar filaments (Ikebe et al., 1988; Katoh and Morita, 1996; Trybus and Lowey, 1988). Many studies using fluorescent-labeled myosin have demonstrated that myosin actively assembles into clusters of bipolar filament at the leading edge of the cell (DeBiasio et al., 1988; Verkhovsky and Borisy, 1993; Verkhovsky et al., 1995). These myosin clusters increase in size and undergo retrograde movement relative to the cell edge in the lamellipodia. The fact that these myosin "spots" appear *de novo* suggests that there is a diffuse pool of myosin in the lamellipodia readily available for regulation and subsequent organization, however, these diffuse myosins may not be detectable with the resolution of fluorescent microscopy. No signal has been identified thus far for the regulation of myosin to form filament clusters.

The fact that $MLCK_{125}$ is active within the lamellipodia makes it a likely candidate. We have shown that there is an increasing gradient of phosphorylated RLC from the leading edge to the large stress fiber network in the cell center, and that MLCK-FIP is active in the lamellipodia. We consistently observe MLCK-FIP associating with actin-like filamentous structures in the lamella. This result places $MLCK_{125}$ at the precise location to activate myosin for subsequent clustering along actin track. Interestingly, attenuating the expression of MLCK using antisense abrogates the extension of lamellipodia and motility in smooth muscle cells in response to platelet-derived growth factor (Kishi et al., 2000), suggesting that MLCK may be involved in lamella formation or maintenance. Although this result is consistent with our finding, the protrusion of lamellipodia is driven mainly by actin polymerization (reviewed in Higgs and Pollard, 2001), thus the precise role played by active myosin at the leading front of a migrating cell remains to be determined. Bipolar myosin II minifilaments aggregate in the lamella to form ribbon-like structures and exert tension required for bundling loosely aligned actin filaments. (Verkhovsky et al., 1995) It is possible that myosin activation leads to contraction at the convergence zone where myosin spots coalesce to form the meshwork of stress fibers (Figure 7). The contraction of the myosin network at this region will exert bi-directional forces both by

pulling the lamellipodia toward the cell center, and on the centroid by pulling the nucleus forward. The fact that large traction force is observed on the small nascent focal complexes at the leading front (Beningo et al., 2001) suggests that these focal complexes are conferring resistance to the $MLCK_{125}$-mediated contractility, therefore converting the contraction into a productive, monodirectional, pulling force between the convergence zone and the nucleus. This is a plausible mechanism by which myosin contractility could work in synergy with actin polymerization to engage the cell in directed movement.

We often observed the lack of significant $MLCK_{125}$ activity at the tail region of motile cells where myosin activity has been postulated to retract cell-substrate adhesion plaques to facilitate movement. The distribution of phosphorylated RLC supports this hypothesis (Matsumura et al., 1998). Therefore, $MLCK_{125}$ may not be the key regulator myosin-mediated tail retraction. In fact recent report showed the Rho kinase is required and sufficient in mediating monocyte tail retraction during transendothelial migration (Worthylake et al., 2001). These observations highlight the value of MLCK-FIP, and exemplify how motile cells compartmentalize these overlapping signaling events.

Bimodal distribution of $MLCK_{125}$ during cytokinesis

Our data show that the enrichment of $MLCK_{125}$ at the midzone of the mitotic spindle during late metaphase precedes its activation. The regulation of $[Ca^{2+}]_4$/calmodulin signal during cytokinesis is biphasic. A sustained elevation of free Ca^{2+} normally begins in anaphase, and persists through daughter cell separation (Tombes and Borisy, 1989). However, this general Ca^{2+} increase can be further fine-tuned by the tight spatiotemporal regulation of calmodulin. During mitosis, calmodulin is concentrated at the spindle poles and the submembrane region (Li et al., 1999). The submembrane pool of calmodulin is redistributed to the equatorial region prior to the formation and contraction of cleavage furrow. More importantly, using a chemical sensor (Torok and Trentham, 1994) that fluoresces upon calmodulin binding to Ca^{2+} and its target, Li *et al.* have shown that only this calmodulin pool at the equator interacts with downstream effector(s).

The $[Ca^{2+}]_4$/calmodulin dynamics fits the MLCK-FIP spectral profile during cytokinesis. There are a few critical implications of detecting $MLCK_{125}$ enrichment at the equator prior to its activation during cleavage contraction. First, it suggests that $MLCK_{125}$ localization is not dependent on $[Ca^{2+}]_4$/calmodulin. In fact, the loss of FRET (indicating the interaction between MLCK and $[Ca^{2+}]_4$/calmodulin) shows no direct correlation with the MLCK-FIP intensity during cytokinesis. These data therefore argue against the possibility that MLCK-FIP artifactually

localizes $MLCK_{125}$ to regions of high $[Ca^{2+}]_4$/calmodulin. Second, our result is contradictory to that of Poperechnaya *et al.* (Poperechnaya et al., 2000) in which GFP-tagged $MLCK_{125}$ did not localize to the cleavage furrow but remained diffuse during cytokinesis. This discrepancy cannot be easily reconciled by immunolocalization as antibody against $MLCK_{125}$ will certainly recognize $MLCK_{210}$. Third, the differential distribution of Ca^{2+} and calmodulin in cultured mammalian cells led to previous postulation that calmodulin may be involved in the positioning of the cleavage furrow (Li et al., 1999). However, the dynamics indicated by MLCK-FIP argues that the contractile machinery may already be in place, and calmodulin provides the localized induction of contractility.

The intensity of $MLCK_{125}$ at the midzone dramatically increases immediately after cleavage furrow formation, while the active $MLCK_{125}$ pool at the opposing poles of the separating daughter cells rises. Detailed analysis of $MLCK_{125}$ intensity suggests that this is a dynamic redistribution event, in which the depleting $MLCK_{125}$ pool at the cleavage furrow is followed co-incidentally by the rise in the polar pool. It is important to note that $[Ca^{2+}]_4$/calmodulin does not show this distribution pattern in previous studies (Li et al., 1999). GFP-calmodulin highlights two high density regions during mitosis. The submembrane pool of calmodulin is redistributed to the equator where it is activated and binds to its target(s), while the other pool prominently decorates the spindle poles. These two pools of calmodulin remain in place even till just prior to the formation of midbody (no further time points are available). The lack of $[Ca^{2+}]_4$/calmodulin at the poles of the daughter cells indicates that $MLCK_{125}$ most likely remains active as the kinase translocates from the equator to the poles. It is unclear what molecular mechanism is responsible for this re-distribution. Examination of myosin distribution using GFP-tagged RLC also reveals this bimodal distribution. Myosin is first concentrated at the equator during late metaphase, but a significant portion of this myosin pool is immediately siphoned to the poles after the constriction of cleavage furrow has occurred (data not shown). It is possible that $MLCK_{125}$ is transported by the same mechanism, if not by the redistributing myosin.

The recruitment of $MLCK_{125}$ to the poles of the daughter cells is consistent with the model that myosin is required for the pulling force at the front. We propose that $MLCK_{125}$ is recruited to the poles where extensive cell spreading resembling lamellipodia is taking place. This event may then mediate myosin activity to facilitate the separation of the two daughter cells in the same way we suggest myosin contractility might pull the nucleus forward during migration.

The data presented here provide strong support for the importance of studying signal transduction with high spatial and temporal resolution. In order to further understand the interplay between $MLCK_{210}$ and $MLCK_{125}$, we are now in the process of generating a FIP-tagged $MLCK_{210}$. This study has documented how cells dynamically recruit MLCK to various cytoskeletal structures and redistribute the kinase when the regulation has taken place. More importantly, MLCK-FIP has demonstrated the lack of direct correlation between intense localization and enzymatic activity, clearly indicating that the localization of a protein cannot be automatically translated into its activity. The FIP technology can easily be expanded to study other $[Ca^{2+}]_4$/calmodulin-depedent proteins *in vivo*, such as calmodulin-dependent kinase II. Approaches similar to those described here to study the dynamics and activation state of other kinases may advance our understanding of the signal transduction that phosphorylate RLC and how they spatially and temporally coordinated to produce directed cell migration.

EXPERIMENTAL PROCEDURES

A. Generating the MLCK-FIP and wt MLCK constructs

Both the BFP and GFP cDNAs PCR amplified from the appropriate vectors of the "Living Colors" GFP vector series purchased from Clontech. Overlapping primers were designed to join the two fluorophores via a linker GTSS**RRKWNKTGHAVRAIGRL<u>SS</u>**TGA. Bold letters denote the $[Ca^{2+}]_4$/calmodulin binding domain derived from MLCK, whereas the rest of the amino acids are linker sequence. Underlined letters represent $MLCK_{125}$ Ser-991 and Ser-992 equivalents. The FIP cDNA was first subcloned into pcDNA3 vector, to generate the pcDNA3/FIP construct. To fuse the $MLCK_{125}$ cDNA in frame into pcDNA3/FIP, murine $MLCK_{125}$ cDNA (GenBank number P29294) was PCR amplified with the downstream primer designed to mutate the stop codon to code for Alanine. $MLCK_{125}$ cDNA was then subcloned into BamH I sites of pcDNA3/FIP. The MLCK-FIP cDNA was sequenced in its entirety to rule out any PCR-related mutation. The final pcDNA3/$MLCK_{125}$-FIP construct contains the murine $MLCK_{125}$ linked to the FIP via a short linker containing the amino acid sequence WDARIVAVES encoded by vector sequence. This construct encodes the 185 kDa MLCK-FIP recombinant protein.

To generate the pcDNA3 vector expressing the wild type $MLCK_{125}$, the murine $MLCK_{125}$ was PCR amplified to engineer the Kpn I and BamH I sites for subcloning into pcDNA3 vector. The positive clones were sequenced to ensure the absence of PCR-related mutation. The construct expresses the 125 kDa wt $MLCK_{125}$.

B. Cell culture and transfection

PTK-2 kangaroo rat epithelial cells (a kind gift by Dr. Robert Goldman, Northwestern University) were cultured in MEM (Gibco-BRL) supplemented with 10% FCS, and 0.1 mM non-essential amino acids. The Normal Rat Kidney (NRK) epithelial cell line was a generous gift from Dr. Yu-Li Wang (University of Masachusetts Medical School, Worcester, MA). NRK cells were cultured in F12 Kaighn's modified medium (Sigma, St. Louis), supplemented with 10% FCS. COS-7 cells were kindly provided by Dr. Kathleen Green (Northwestern University) and were maintained in DMEM supplemented with 10% FCS. All cell lines were maintained in an atmosphere of 5% CO_2 at 37°C.

Transfection was performed by electroporation. Cells grown on 10 cm plates were trypsinized and pelleted by centrifugation. The cell pellets were resuspended in 1 ml appropriate medium. 200 μl of the resuspended cells were mixed with 7-10 μg DNA containing 13 μg sheared salmon sperm DNA and electroporated in 4 mm cuvettes using Bio Rad Gene Pulser electroporator set at 200 ohms, 960 μFD, 250 V. Using this method, the resulting transfection efficiencies were high (70-90%) for most cell types at a wide range of cell density except NRK cells, in which about 10-15% could be transfected. Peak protein expression levels observed 18-24 hours post-transfection for all cell lines.

C. Reagents, proteins and antibodies

Polyclonal rabbit anti-MLCK antibody and purified $MLCK_{125}$ were generously provided by Dr. Robert Wysolmerski (St. Louis University, St. Louis, MO). Ionomycin was purchased from Calbiochem and prepared according to the manufacturer's protocol. Protein-A sepharose was purchased from Pharmacia. pp2b rabbit polyclonal antibody specific for Ser-19-phosphorylated RLC was obtained from Dr. Fumio Matsumura. Monoclonal anti-myosin heavy chain antibody is purchased from Covance. Texas Red-conjugated goat anti-mouse IgM and Cy5-conjugated donkey anti-rabbit IgG were purchased from Jackson ImmunoResearch Laboratories. Calmodulin was purchased from Calbiochem.

D. Protein expression and purification

Myosin II RLC cDNA was cloned into pET14b vector (Novagen) to allow for the expression of His-tagged RLC, and protein expression was induced in BL21 by 0.4 mM IPTG for three hours. Bacterial pellet was lysed in Lysis Buffer A (5 mM Imidazole, 0.5 NaCl, 20 mM Tris-HCl, pH 7.9) containing 6 M Urea and protease inhibitors. Following sonication, cell lysate was pre-cleared by 20,000 *g* centrifugation, and loaded onto His-Bind column (Novagen) pre-

equilibrated with the same buffer. After washing the column with Washing Buffer A (60 mM Imidazole, 0.5 M NaCl, 20 mM Tris-HCl, pH 7.9), protein was eluted using Elution Buffer A (500 mM Imidazole, 250 mM NaCl, 10 mM Tris-HCl, pH 7.9). The eluted protein was dialyzed against Dialysis Buffer A (20 mM MOPS, pH 7.2, 250 mM NaCl, 1 mM $CaCl_2$, 1 mM $MgCl_2$) with stepwise decrease of imidazole concentration from 500 mM to 250 mM. Lower imidazole concentration resulted in massive protein precipitation. Cleaving the His tag did not eradicate the precipitation problem.

MLCK-FIP and wt MLCK were over-expressed in COS-7 cells for purification. Cell lysates were collected from sixteen confluent 10 cm circular cell culture dishes. Cells were lysed in 35 ml of Lysis Buffer B (10 mM MOPS, pH 6.8, 5 mM $MgCl_2$, 1.25 mM EGTA, 1 mM EDTA, 10% glycerol, 1% NP-40) containing protease inhibitors. Lysates were sonicated briefly in sonicator waterbath and pre-cleared with 50,000 *g* centrifugation, and purified using Mono-Q ion exchange chromatography, pre-equilibrated with Lysis Buffer B without NP-40 and glycerol. The column was washed with two volumes of equilibration buffer and the proteins eluted against a gradient of 0 to 600 mM NaCl in Elution Buffer B (10 mM MOPS, pH 6.8, 5 mM $MgCl_2$, 1.25 mM EGTA, 1 mM EDTA). Analysis of the elution profile showed that MLCK-FIP and wt MLCK were reproducibly eluted three fractions apart from one another, thus allowing us to separate MLCK-FIP from endogenous wt MLCK.

E. *In vitro* FRET analysis

In vitro spectrofluorimetric analysis of MLCK-FIP was performed using an AMINCO Bowman Series 2 Luminescence Spectrometer. An excitation wavelength of 380 nm was used throughout the experiment. Purified MLCK-FIP was assayed in 1 ml reaction mixture containing 20 mM MOPS Buffer, pH 7.2, 10 mM NaCl, 1 mM EDTA, 1 mM EGTA, and 1 μM calmodulin. Standard $CaCl_2$ solution is added to the cuvette to titrate the effects of increasing $[Ca^{2+}]_4$/calmodulin. The free Ca^{2+} available for binding to calmodulin is calculated by MaxChelator program, taking into account all divalent cations and their chelators in the buffer. An emission scan from 430 nm to 540 nM was performed with each addition of $CaCl_2$.

F. RLC Phosphorylation

To examine compare the rate of phosphate incorporation into RLC catalyzed by MLCK-FIP with that of wt MLCK, the recombinant proteins were transiently over-expressed in COS-7 cells, and immunoprecipitated using rabbit polyclonal anti-MLCK antibody. The amount of immunoprecipitated MLCK was estimated by comparing the densitometric units of the MLCK

bands on immunoblot to that of a standard curve set up by varying amount of recombinant $MLCK_{125}$. Immunoprecipitate containing 1 μg kinase was used in the *in vitro* kinase assay. The fact that our recombinant RLC precipitates at low salt and very high protein concentration precludes the accurate determination of Vmax and Km by conventional method. Instead we compared the rate of phosphorylation by MLCK-FIP and wt MLCK at three substrate concentrations. Kinase assay was performed in 25 mM Tris-HCl, pH 7.5, 5 mM $MgCl_2$, 1mM DTT, 0.5 mM $CaCl_2$, 100 mM KCl, and 1 μM calmodulin. Specific activity of ^{32}P-γ-ATP was 4000 cpm/pmole. 5 μl of the reaction was removed at the indicated time points and spotted onto Whatman P81 ion exchange paper, and the reaction stopped by ice-cold 10% trichloroacetic acid containing 2% sodium pyrophosphate. The papers were washed four times in ice-cold acetone, heated to 80°C for 15 minutes, and washed once with acetone to remove heat-labile phosphate. The samples were then counted in a scintillation counter.

G. Live cell imaging

Live cell imaging was carried out on Zeiss Axiovert S100-TV inverted fluorescent microscope. Rapid switching of fluorescent wavelength was accomplished by emission and excitation filter wheels controlled by Sutter Instruments Lambda 10 controller, and the shutters controlled Uniblitz VMM-D1 shutter drivers. Digital fluorescent images were captured by Micromax cooled CCD camera (Princeton Instruments) with a 512 X 512 camera chip. Filter wheels are equipped with bandpass filters for BFP and GFP with a stationary dual beamsplitter for BFP and GFP located in the filter block. Filters were purchased from Chroma. Live cells were imaged in a Bioptech FCS2 closed chamber system maintained at 37°C, with a chamber thickness of 0.75 mm. In order to reduce the background fluorescence as well as to image cell under no CO_2 condition, the cell medium was mixed with equal volume of Leibovitz's medium without Phenol Red (Gibco BRL) supplemented with 10% FCS, and fresh medium perfused at 0.1 ml/min into the chamber during imaging.

Cell images were taken using MetaMorph 4.5 (Universal Imaging) software. The images were taken with 200 – 300 ms exposure with approximately 50 ms interval between the numerator F_{FRET} and the denominator F_{GFP} images. Ratio images were constructed by displaying the ratio in 16 different color hues with the lowest ratio (MLCK active) displayed at the blue end of the ratio spectrum. Using the intensity of the denominator (which served as the internal control irrespective of FRET), the ratio colors were displayed in sixteen different intensity levels by the Intensity Modulatory Display mode (Figure #). Therefore, depending on the enrichment and the activation state of MLCK-FIP at any given subcellular region, the color of

the ratio denotes the relative extent at which MLCK-FIP associates with $[Ca^{2+}]_4$/calmodulin, while the intensity of that ratio color represents the amount of MLCK-FIP being localized by the cell. To highlight the dynamic recruitment of $MLCK_{125}$ to cytoskeletal structures, FRET ratio was plotted against the intensity profile, whereby the pixel intensity was represented by line height, and the FRET ratio depicted by the line color. We have avoided cells with saturated pixels to minimize error on ratio calculation.

To correlate the relative activity of MLCK-FIP with the extent of RLC phosphorylation *in vivo*, PTK-2 cells transiently expressing MLCK-FIP was plated on grided coverslips. The ratio images of MLCK-FIP were obtained as described, and the cells were immediately fixed as described previously. The coverslips was blocked with PBS containing 0.1% BSA and 1:20 dilution of normal goat serum. Double immunofluorescence was performed with anti-myosin mAb and pp2b polyclonal anti-phosphorylated RLC antibody. Primary antibody incubation performed at 37°C for one hour. After washing in PBS, the secondary antibody was carried out at 37°C for 30 minutes with Texas Red-conjugated goat anti-mouse IgM, and Cy5-conjugated donkey anti-rabbit IgG. Immunolocalization images were taken with Zeiss LSM 510 confocal microscope and ratio of the images performed on MetaMorph 4.5.

FIGURE LEGENDS

Figure 1. MLCK-FIP is a FRET-based $[Ca^{2+}]_4$/calmodulin sensor that maintain kinase activity and regulation similar to wt MLCK.

(A) *Schematic diagram of MLCK-FIP*. The fluorescent indicator protein (FIP) is comprised of a BFP linked to a GFP via a $[Ca^{2+}]_4$/calmodulin-binding domain derived from MLCK. In the absence of $[Ca^{2+}]_4$/calmodulin, the coiled $[Ca^{2+}]_4$/calmodulin binding domain allows FRET between the fluorophores. When $[Ca^{2+}]_4$/calmodulin (yellow cylinder) is present, it will activate MLCK and bind in between the fluorophores and disrupt FRET. (B) *MLCK-FIP shows $[Ca^{2+}]_4$/calmodulin dependent kinase activity.* Lysates from COS-7 cells transiently expressing MLCK-FIP or wt MLCK were compared for the $[Ca^{2+}]_4$/calmodulin-dependent kinase activity to phosphorylate RLC. Lysate from mock-transfected cells served as negative control. Endogenous kinase activity was evident only prolonged exposure of the autoradiograph. (C) *MLCK-FIP phosphorylates RLC with similar rate as wt MLCK.* The RLC phosphorylation rate of immunoprecipitated MLCK-FIP and wt MLCK were compared at 3 substrate concentrations. Amount of immunoprecipitated kinase was normalized against a standard curve of known protein concentrations immunoblotted by anti-MLCK pAb (bottom panel).

Figure 2. MLCK-FIP detects $[Ca^{2+}]_4$/calmodulin changes *in vitro* and *in vivo*.

(A) Partially purified MLCK-FIP in buffer containing 1 μM calmodulin was exposed to increasing amount of free Ca^{2+}. Emission scan from 430 nm to 540 nm excited at 380 nm was obtained after each addition of $CaCl_2$. (B) COS-7 cells overexpressing MLCK-FIP were treated with 1 μM ionomycin, and ratio imaging performed to monitor the $[Ca^{2+}]_4$/calmodulin binding to MLCK-FIP. Relative state of $[Ca^{2+}]_4$/calmodulin binding (representing MLCK activity) was displayed according to the ratio bar (bottom panel). Red color (high ratio) represents low $[Ca^{2+}]_4$/calmodulin binding state, while blue (low ratio) shows high $[Ca^{2+}]_4$/calmodulin binding state, indicative of active MLCK.

Figure 4. MLCK-FIP associates with stress fibers and highlights areas of RLC phosphorylation.

(A) Co-localization of MLCK-FIP to rhodamine phallodin-stained stress fibers. (B) Relative distribution of RLC phosphorylation was obtained by determining the ratio of phosphorylated RLC to total myosin (right panel). Ratio image is displayed according to the ratio bar (right bottom panel). High RLC/total myosin ratio is indicated by red. Left panel shows the MLCK-FIP localization and activity. Arrow heads show phosphorylated RLC decorating stress fibers. Arrow highlights region of lamellipodia with high kinase activity co-localizes with myosin spots. Note the increasing gradient of phosphorylation toward the cell center. Bar, 5 μm.

Figure 3. Transient recruitment and activation of $MLCK_{125}$ along contracting stress fibers.

Ratio images of two contracting cells (panels A – D; and E – H) were displayed by their intensity profiles. The intensity of MLCK-FIP is represented by the peak height (high peaks indicate enrichment of MLCK) while the MLCK-FIP $[Ca^{2+}]_4$/calmodulin-binding state is displayed by the color. Red color (high ratio) represents inactive kinase, while blue indicates $[Ca^{2+}]_4$/calmodulin-bound kinase. Arrows trace the process of recruiting diffuse MLCK to stress fibers, arrow heads show *in situ* activation of MLCK-FIP.

Figure 5 $MLCK_{125}$ is activated in the lamellipodia.

MLCK-FIP shows the binding of $[Ca^{2+}]_4$/calmodulin to MLCK within the lamellipodia. Ratio images were constructed for a migrating MDCK epithelial cells. Relative MLCK active is represented by the same ratio bar used in figure 3. Red and blue line trace the outlines of the cell at the beginning and the end of the image series, respectively.

Figure 6 $MLCK_{125}$ shows bimodal distribution during cell division.

The dynamics of $MLCK_{125}$ localization and state of activation during cell division was monitored in NRK cell using MLCK-FIP. The relative intensity and activity of MLCK at regions 1 – 3 are represented in graphs at the bottom panel.

Figure 7 A model for myosin contraction as a pulling force in motility.

A cartoon illustration of how myosin contraction at the front of the nucleus may work synergistically with actin polymerization to facilitate movement. Myosin contraction at the convergence zone generates a bi-directional pulling force, acting on both the leading edge and

the cell centroid. The pulling force at the leading front is rendered non-productive by the nascent focal adhesions, turning myosin contraction into a productive mono-directional that pulls the centroid forward. Rho kinase-activated myosin also acts at the tail to peel off focal contacts during motility.

REFERENCES

Amano, M., Ito, M., Kimura, K., Fukata, Y., Chihara, K., Nakano, T., Matsuura, Y., and Kaibuchi, K. (1996). Phosphorylation and activation of myosin by Rho-associated kinase (Rho- kinase). J Biol Chem *271*, 20246-9.

Beningo, K. A., Dembo, M., Kaverina, I., Small, J. V., and Wang, Y. L. (2001). Nascent focal adhesions are responsible for the generation of strong propulsive forces in migrating fibroblasts. J Cell Biol *153*, 881-8.

Birukov, K. G., Schavocky, J. P., Shirinsky, V. P., Chibalina, M. V., Van Eldik, L. J., and Watterson, D. M. (1998). Organization of the genetic locus for chicken myosin light chain kinase is complex: multiple proteins are encoded and exhibit differential expression and localization. J Cell Biochem *70*, 402-13.

Chew, T. L., Masaracchia, R., and Wysolmerski, R. (1998). Phosphorylation of non-muscle myosin II regulatory light chain by p21- activated kinase (gamma-PAK). J Muscle Res Cell Motil *19*, 839-54.

Chrzanowska-Wodnicka, M., and Burridge, K. (1996). Rho-stimulated contractility drives the formation of stress fibers and focal adhesions. J Cell Biol *133*, 1403-15.

de Lanerolle, P., Adelstein, R. S., Feramisco, J. R., and Burridge, K. (1981). Characterization of antibodies to smooth muscle myosin kinase and their use in localizing myosin kinase in nonmuscle cells. Proc Natl Acad Sci U S A *78*, 4738-42.

DeBiasio, R. L., Wang, L. L., Fisher, G. W., and Taylor, D. L. (1988). The dynamic distribution of fluorescent analogues of actin and myosin in protrusions at the leading edge of migrating Swiss 3T3 fibroblasts. J Cell Biol *107*, 2631-45.

Gallagher, P. J., and Herring, B. P. (1991). The carboxyl terminus of the smooth muscle myosin light chain kinase is expressed as an independent protein, telokin. J Biol Chem *266*, 23945-52.

Garcia, J. G., Davis, H. W., and Patterson, C. E. (1995). Regulation of endothelial cell gap formation and barrier dysfunction: role of myosin light chain phosphorylation. J Cell Physiol *163*, 510-22.

Goeckeler, Z. M., Masaracchia, R. A., Zeng, Q., Chew, T. L., Gallagher, P., and Wysolmerski, R. B. (2000). Phosphorylation of myosin light chain kinase by p21-activated kinase PAK2. J Biol Chem *275*, 18366-74.

Goeckeler, Z. M., and Wysolmerski, R. B. (1995). Myosin light chain kinase-regulated endothelial cell contraction: the relationship between isometric tension, actin polymerization, and myosin phosphorylation. J Cell Biol *130*, 613-27.

Guerriero, V., Jr., Rowley, D. R., and Means, A. R. (1981). Production and characterization of an antibody to myosin light chain kinase and intracellular localization of the enzyme. Cell *27*, 449-58.

Higgs, H. N., and Pollard, T. D. (2001). Regulation of actin filament network formation through Arp2/3 complex: Activation by a Diverse Array of Proteins. Annu Rev Biochem *70*, 649-676.

Ikebe, M., and Hartshorne, D. J. (1985). Phosphorylation of smooth muscle myosin at two distinct sites by myosin light chain kinase. J Biol Chem *260*, 10027-31.

Ikebe, M., Hartshorne, D. J., and Elzinga, M. (1986). Identification, phosphorylation, and dephosphorylation of a second site for myosin light chain kinase on the 20,000-dalton light chain of smooth muscle myosin. J Biol Chem *261*, 36-9.

Ikebe, M., Hartshorne, D. J., and Elzinga, M. (1987). Phosphorylation of the 20,000-dalton light chain of smooth muscle myosin by the calcium-activated, phospholipid-dependent protein kinase. Phosphorylation sites and effects of phosphorylation. J Biol Chem *262*, 9569-73.

Ikebe, M., Koretz, J., and Hartshorne, D. J. (1988). Effects of phosphorylation of light chain residues threonine 18 and serine 19 on the properties and conformation of smooth muscle myosin. J Biol Chem *263*, 6432-7.

Ikebe, M., and Reardon, S. (1990). Phosphorylation of smooth myosin light chain kinase by smooth muscle Ca2+/calmodulin-dependent multifunctional protein kinase. J Biol Chem *265*, 8975-8.

Katoh, K., Kano, Y., Amano, M., Onishi, H., Kaibuchi, K., and Fujiwara, K. (2001). Rho-kinase--mediated contraction of isolated stress fibers. J Cell Biol *153*, 569-84.

Katoh, T., and Morita, F. (1996). Roles of light chains in the activity and conformation of smooth muscle myosin. J Biol Chem *271*, 9992-6.

Kishi, H., Mikawa, T., Seto, M., Sasaki, Y., Kanayasu-Toyoda, T., Yamaguchi, T., Imamura, M., Ito, M., Karaki, H., Bao, J., Nakamura, A., Ishikawa, R., and Kohama, K. (2000). Stable transfectants of smooth muscle cell line lacking the expression of myosin light chain kinase and their characterization with respect to the actomyosin system. J Biol Chem *275*, 1414-20.

Li, C. J., Heim, R., Lu, P., Pu, Y., Tsien, R. Y., and Chang, D. C. (1999). Dynamic redistribution of calmodulin in HeLa cells during cell division as revealed by a GFP-calmodulin fusion protein technique. J Cell Sci *112*, 1567-77.

Lin, P., Luby-Phelps, K., and Stull, J. T. (1997). Binding of myosin light chain kinase to cellular actin-myosin filaments. J Biol Chem *272*, 7412-20.

Lin, P., Luby-Phelps, K., and Stull, J. T. (1999). Properties of filament-bound myosin light chain kinase. J Biol Chem *274*, 5987-94.

Matsumura, F., Ono, S., Yamakita, Y., Totsukawa, G., and Yamashiro, S. (1998). Specific localization of serine 19 phosphorylated myosin II during cell locomotion and mitosis of cultured cells. J Cell Biol *140*, 119-29.

Mishima, M., and Mabuchi, I. (1996). Cell cycle-dependent phosphorylation of smooth muscle myosin light chain in sea urchin egg extracts. J Biochem (Tokyo) *119*, 906-13.

Nishikawa, M., Shirakawa, S., and Adelstein, R. S. (1985). Phosphorylation of smooth muscle myosin light chain kinase by protein kinase C. Comparative study of the phosphorylated sites. J Biol Chem *260*, 8978-83.

Payne, M. E., Elzinga, M., and Adelstein, R. S. (1986). Smooth muscle myosin light chain kinase. Amino acid sequence at the site phosphorylated by adenosine cyclic 3',5'-phosphate-dependent protein kinase whether or not calmodulin is bound. J Biol Chem *261*, 16346-50.

Poperechnaya, A., Varlamova, O., Lin, P., Stull, J. T., and Bresnick, A. R. (2000). Localization and activity of myosin light chain kinase isoforms during the cell cycle. J Cell Biol *151*, 697-708.

Romoser, V. A., Hinkle, P. M., and Persechini, A. (1997). Detection in living cells of Ca2+-dependent changes in the fluorescence emission of an indicator composed of two green fluorescent protein variants linked by a calmodulin-binding sequence. A new class of fluorescent indicators. J Biol Chem *272*, 13270-4.

Sanders, L. C., Matsumura, F., Bokoch, G. M., and de Lanerolle, P. (1999). Inhibition of myosin light chain kinase by p21-activated kinase. Science *283*, 2083-5.

Satterwhite, L. L., Lohka, M. J., Wilson, K. L., Scherson, T. Y., Cisek, L. J., Corden, J. L., and Pollard, T. D. (1992). Phosphorylation of myosin-II regulatory light chain by cyclin-p34cdc2: a mechanism for the timing of cytokinesis. J Cell Biol *118*, 595-605.

Sellers, J. R., Pato, M. D., and Adelstein, R. S. (1981). Reversible phosphorylation of smooth muscle myosin, heavy meromyosin, and platelet myosin. J Biol Chem *256*, 13137-42.

Tansey, M. G., Word, R. A., Hidaka, H., Singer, H. A., Schworer, C. M., Kamm, K. E., and Stull, J. T. (1992). Phosphorylation of myosin light chain kinase by the multifunctional calmodulin-dependent protein kinase II in smooth muscle cells. J Biol Chem *267*, 12511-6.

Tombes, R. M., and Borisy, G. G. (1989). Intracellular free calcium and mitosis in mammalian cells: anaphase onset is calcium modulated, but is not triggered by a brief transient. J Cell Biol *109*, 627-36.

Torok, K., and Trentham, D. R. (1994). Mechanism of 2-chloro-(epsilon-amino-Lys75)-[6-[4-(N,N- diethylamino)phenyl]-1,3,5-triazin-4-yl]calmodulin interactions with smooth muscle myosin light chain kinase and derived peptides. Biochemistry *33*, 12807-20.

Trybus, K. M., and Lowey, S. (1988). The regulatory light chain is required for folding of smooth muscle myosin. J Biol Chem *263*, 16485-92.

Tsien, R. Y., and Harootunian, A. T. (1990). Practical design criteria for a dynamic ratio imaging system. Cell Calcium *11*, 93-109.

Turbedsky, K., Pollard, T. D., and Bresnick, A. R. (1997). A subset of protein kinase C phosphorylation sites on the myosin II regulatory light chain inhibits phosphorylation by myosin light chain kinase. Biochemistry *36*, 2063-7.

Verkhovsky, A. B., and Borisy, G. G. (1993). Non-sarcomeric mode of myosin II organization in the fibroblast lamellum. J Cell Biol *123*, 637-52.

Verkhovsky, A. B., Svitkina, T. M., and Borisy, G. G. (1995). Myosin II filament assemblies in the active lamella of fibroblasts: their morphogenesis and role in the formation of actin filament bundles. J Cell Biol *131*, 989-1002.

Worthylake, R. A., Lemoine, S., Watson, J. M., and Burridge, K. (2001). RhoA is required for monocyte tail retraction during transendothelial migration. J Cell Biol *154*, 147-160.

Wysolmerski, R. B., and Lagunoff, D. (1991). Regulation of permeabilized endothelial cell retraction by myosin phosphorylation. Am J Physiol *261*, C32-40.

Zeng, Q., Lagunoff, D., Masaracchia, R., Goeckeler, Z., Cote, G., and Wysolmerski, R. (2000). Endothelial cell retraction is induced by PAK2 monophosphorylation of myosin II. J Cell Sci *113*, 471-82.

Figure 1

A

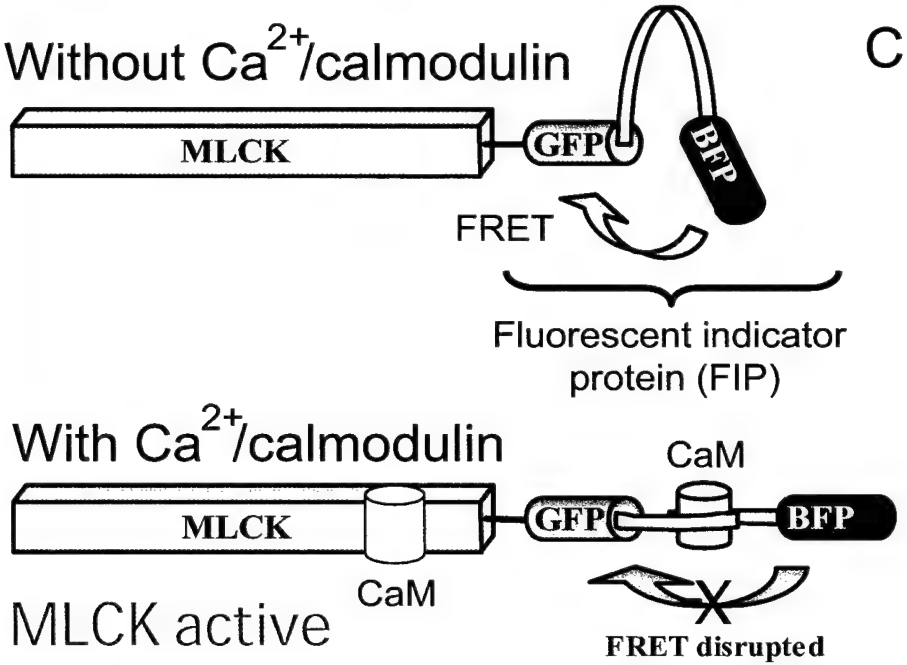
Without Ca2+/calmodulin
MLCK
GFP
BFP
FRET
Fluorescent indicator protein (FIP)
With Ca2+/calmodulin
CaM
MLCK
GFP
BFP
CaM
MLCK active
FRET disrupted

B

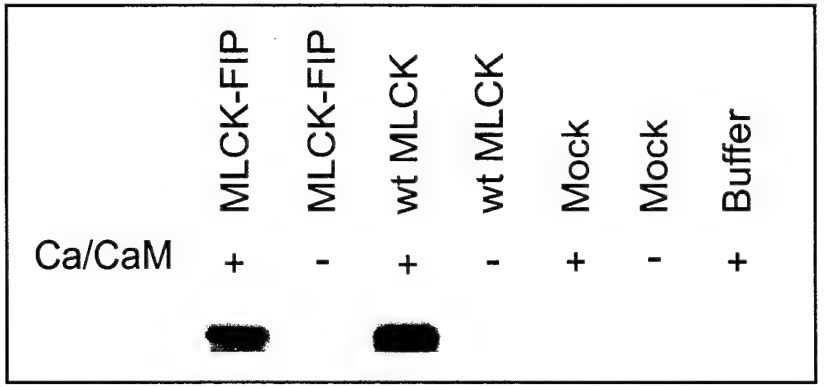
MLCK-FIP
MLCK-FIP
wt MLCK
wt MLCK
Mock
Mock
Buffer
Ca/CaM
+
-
+
-
+
-
+

C

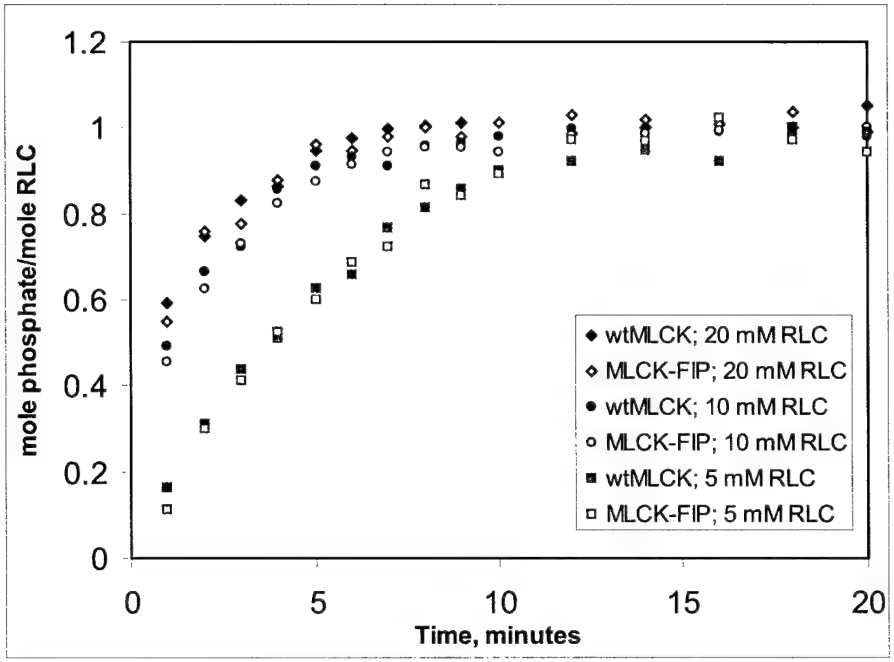
mole phosphate/mole RLC
Time, minutes
wtMLCK; 20 mM RLC
MLCK-FIP; 20 mM RLC
wtMLCK; 10 mM RLC
MLCK-FIP; 10 mM RLC
wtMLCK; 5 mM RLC
MLCK-FIP; 5 mM RLC

Figure 2

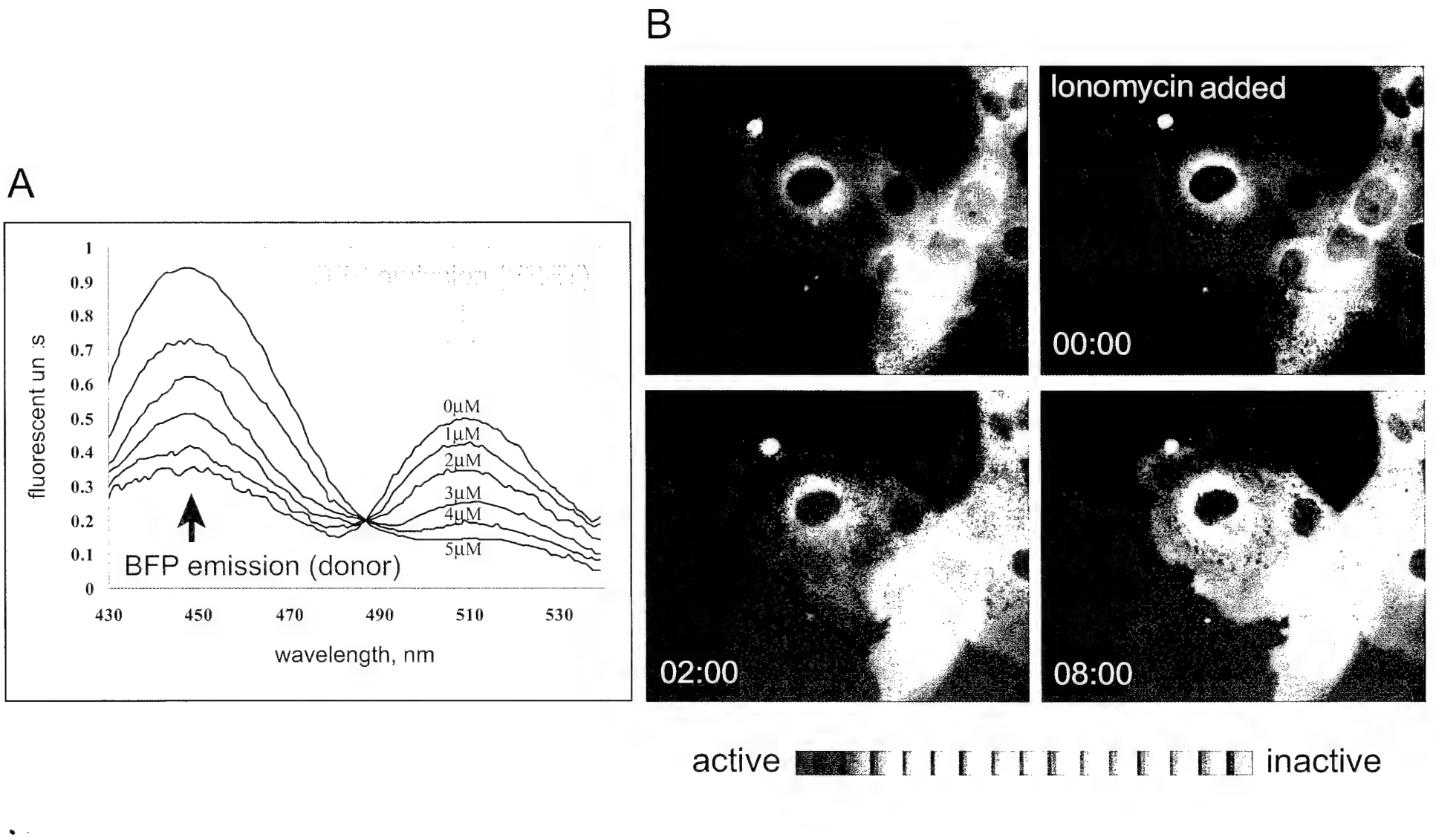
A
fluorescent units
1
0.9
0.8
0.7
0.6
0.5
0.4
0.3
0.2
0.1
0
0μM
1μM
2μM
3μM
4μM
5μM
BFP emission (donor)
430
450
470
490
510
530
wavelength, nm
B
Ionomycin added
00:00
02:00
08:00
active
inactive

Figure 3

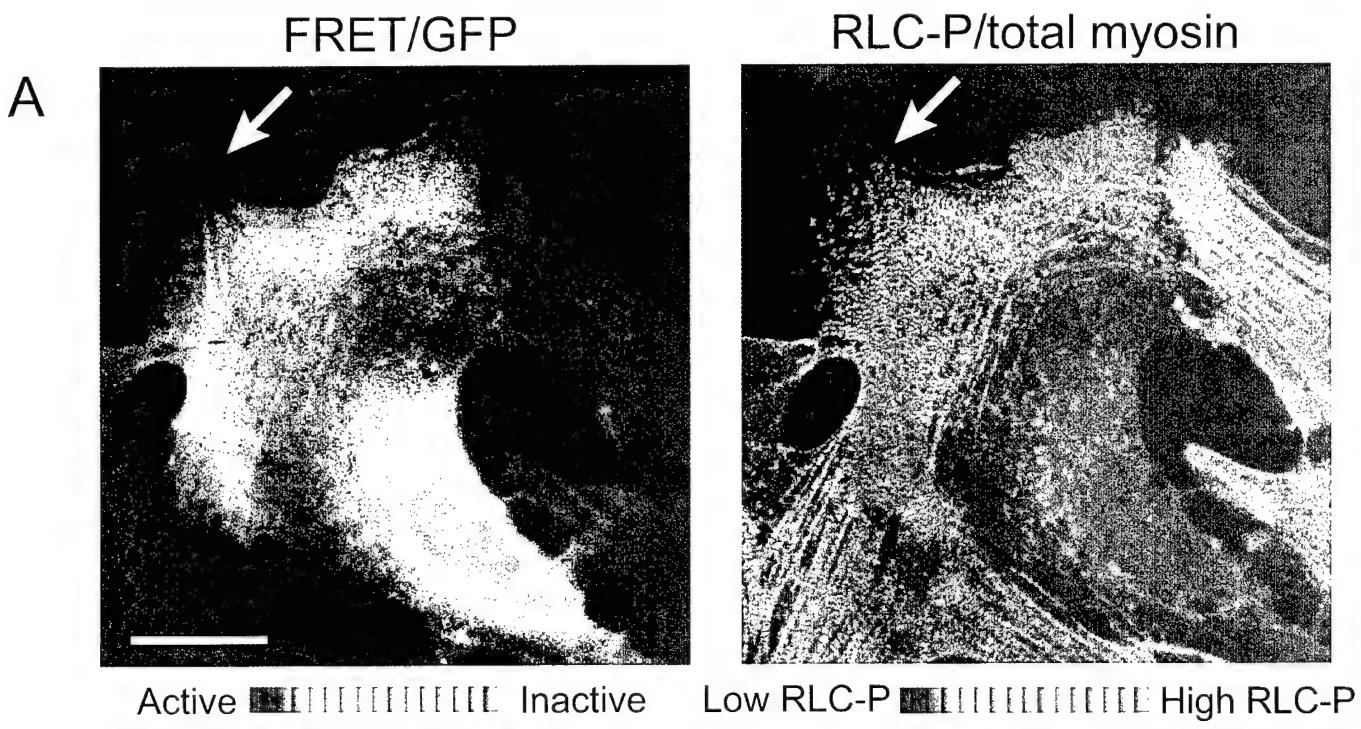
FRET/GFP
RLC-P/total myosin
A
Active
Inactive
Low RLC-P
High RLC-P

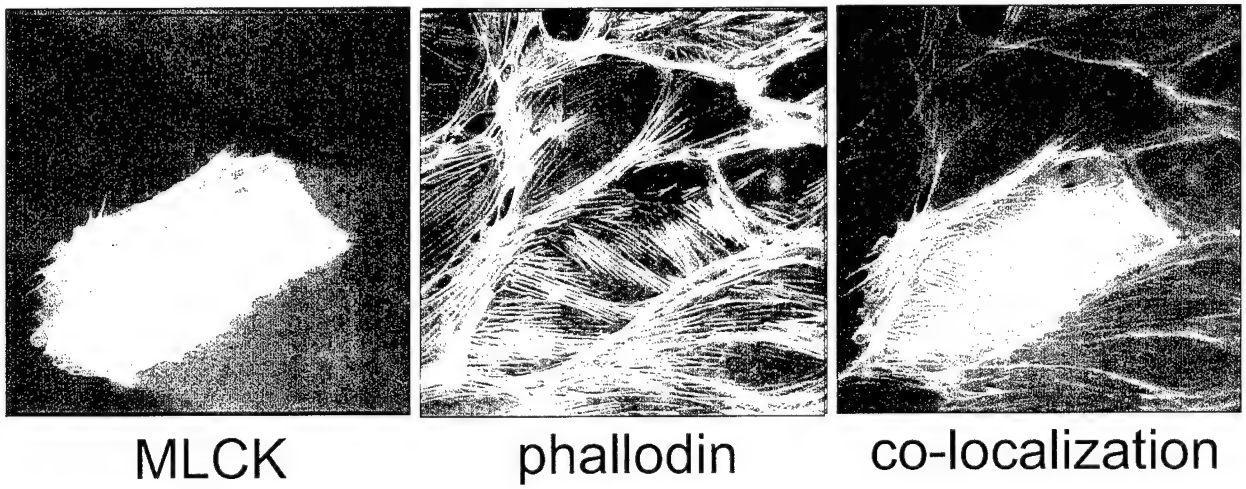
B
MLCK
phallodin
co-localization

Figure 4

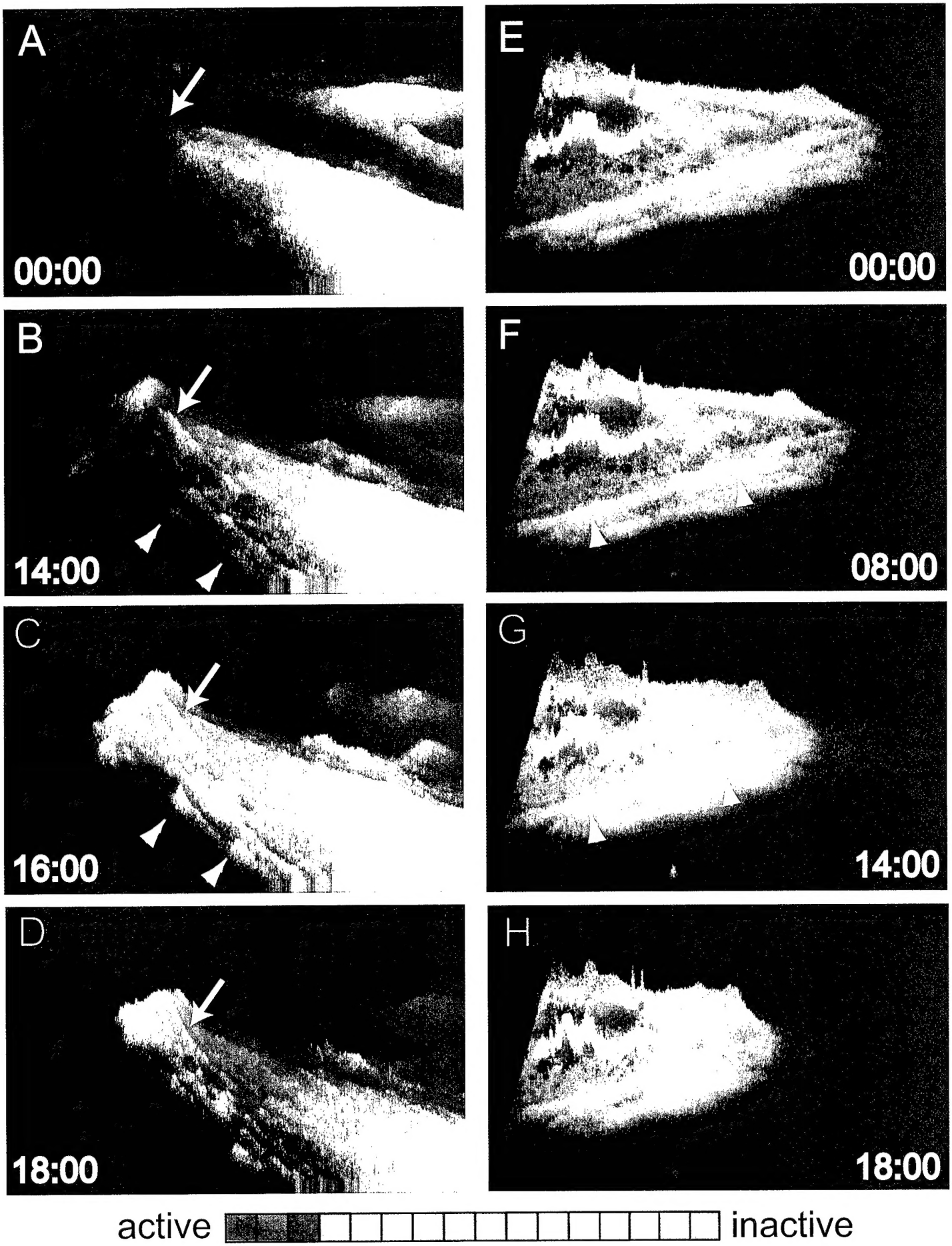
A
00:00
B
14:00
C
16:00
D
18:00
E
00:00
F
08:00
G
14:00
H
18:00
active
inactive

Figure 5

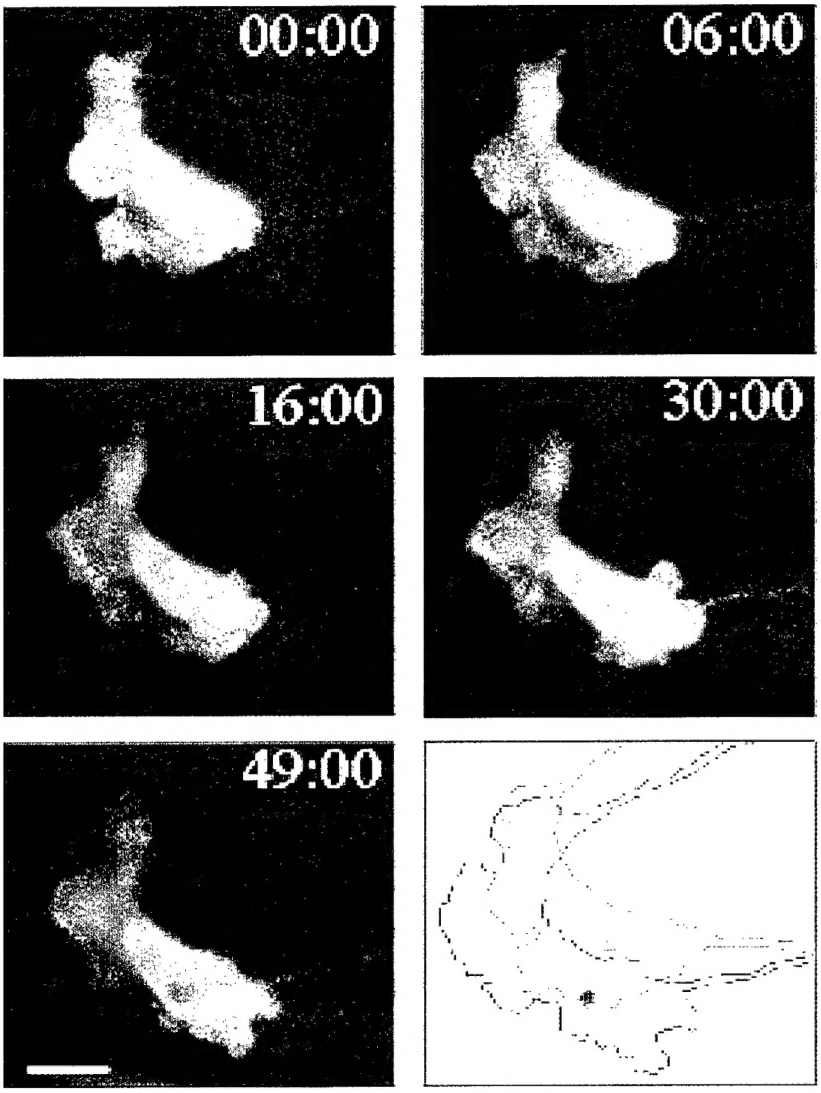

Figure 6

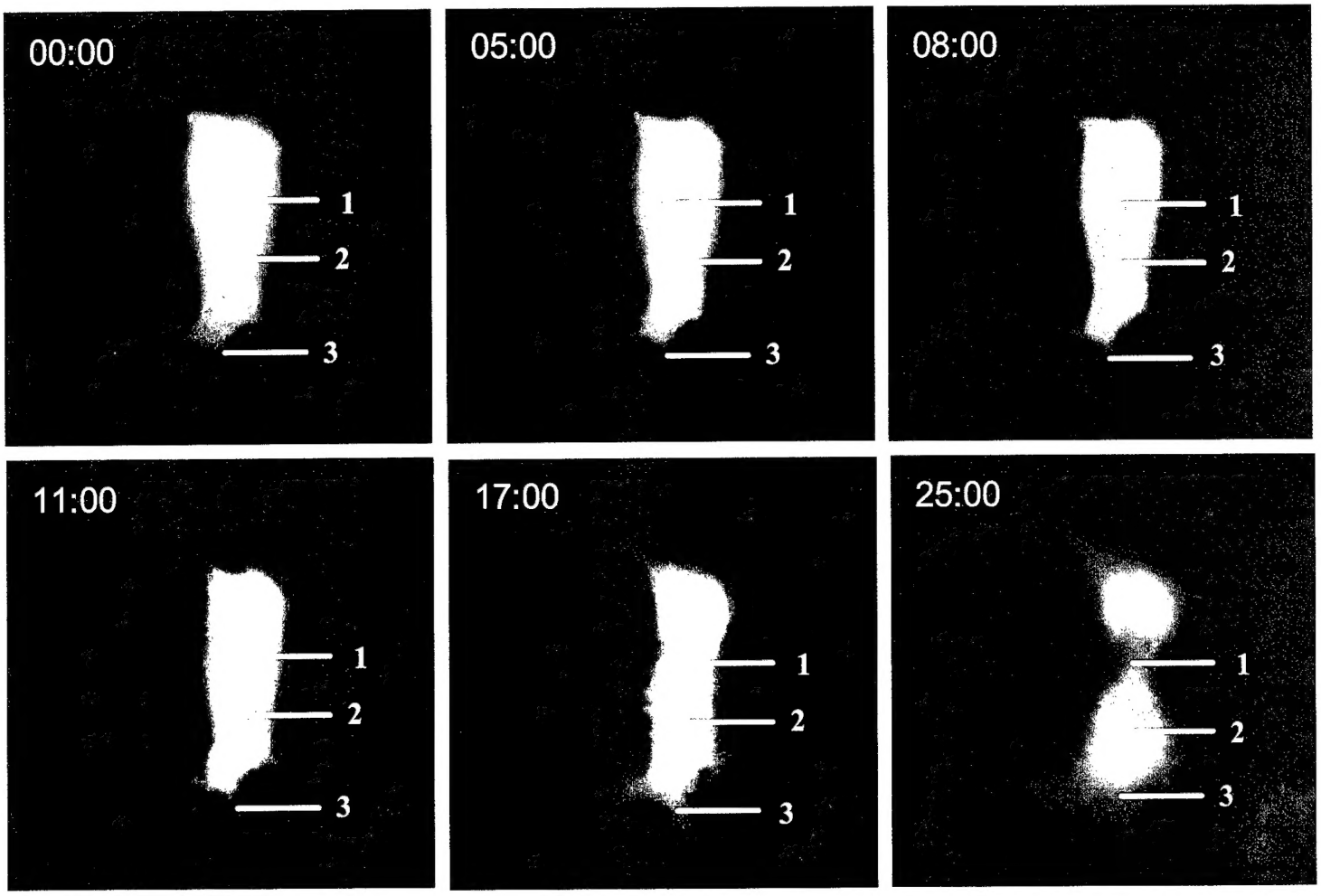

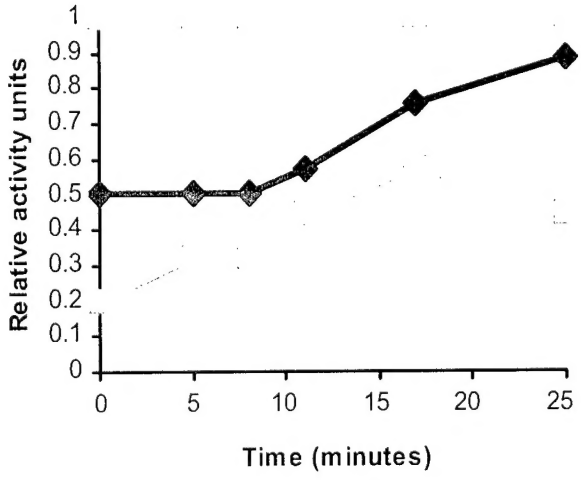

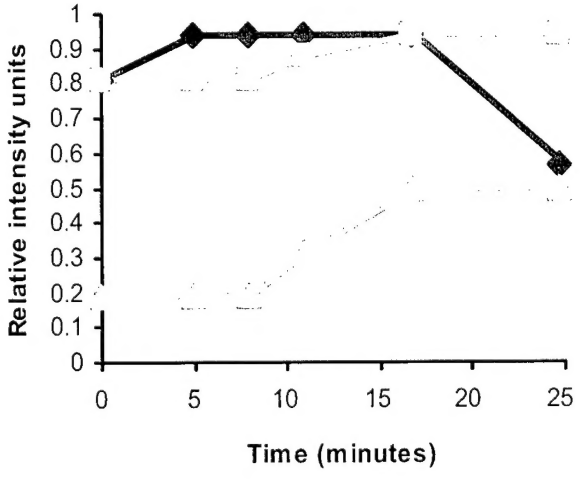

Region 1

Region 2

Region 3

Figure 7

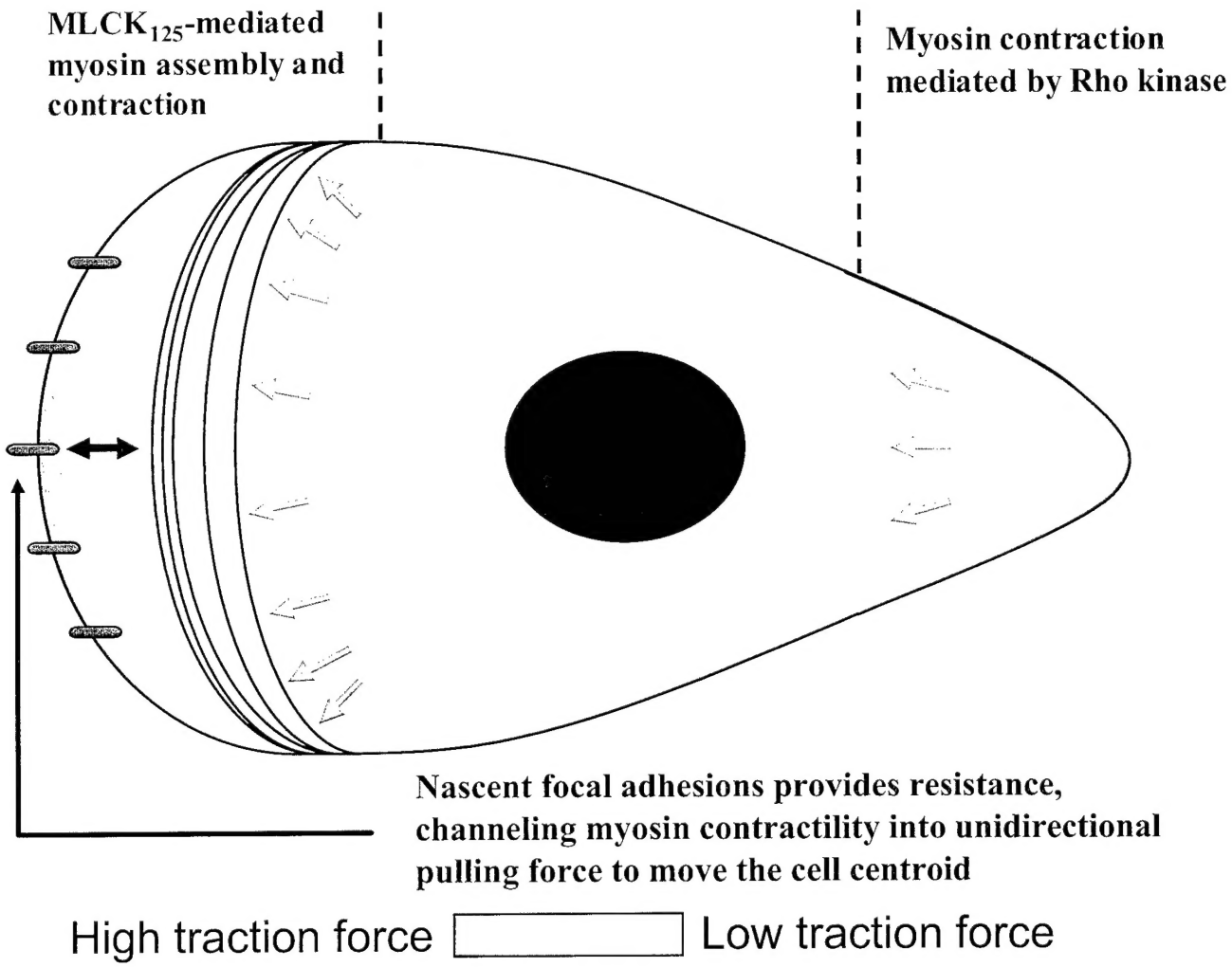
MLCK125-mediated myosin assembly and contraction
Myosin contraction mediated by Rho kinase
Nascent focal adhesions provides resistance, channeling myosin contractility into unidirectional pulling force to move the cell centroid
High traction force
Low traction force